

# POLITECNICO DI TORINO

Department of Mechanical Engineering  
Department of Energy

**Master of Science  
in Mechanical Engineering**

## **CFD SIMULATION OF A HEAVY- DUTY GAS TURBINE COMBUSTOR**



### **Supervisors**

Prof.ssa Daniela Anna Misul  
Prof. Mirko Baratta  
Dott. Ing. Prashant Goel  
Dott. Ing. Mohsen MosayebNezhad

### **Candidate**

Daniele Delia

A.Y. 2018/2019



# INDEX

<b>1</b>	<b>INTRODUCTION</b>	<b>8</b>
1.1	PURPOSE OF THE STUDY	8
1.2	ETHOSENERGY S.P.A.	9
1.3	GAS TURBINES	10
1.4	THESIS OVERVIEW	12
<b>2</b>	<b>THEORETICAL BACKGROUND</b>	<b>15</b>
2.1.1	<i>General continuity equations</i>	15
2.1.2	<i>Thermal and caloric equation of state</i>	17
2.1.3	<i>Transport Models</i>	19
2.2	COMBUSTION CHEMISTRY	21
2.3	TURBULENCE MODELING	22
2.3.1	<i>Reynolds-Averaged Navier-Stokes (RANS) Equations</i>	24
2.3.2	<i>Turbulence Models</i>	26
2.3.3	<i>RNG <math>k</math>-<math>\epsilon</math> Turbulence Model</i>	26
<b>3</b>	<b>CONVERGE CFD TOOL</b>	<b>31</b>
3.1.1	<i>Discretization methods</i>	32
3.1.2	<i>Solution procedure</i>	33
3.1.3	<i>Piso algorithm</i>	35
3.1.4	<i>CFL number</i>	36
3.1.5	<i>Steady-state solver</i>	37
3.2	BOUNDARY CONDITIONS	38
3.3	MESH GENERATION	39
3.3.1	<i>Grid scaling</i>	41
3.3.2	<i>Fixed embedding</i>	41
3.3.3	<i>Adaptive mesh refinement (AMR)</i>	43
3.4	COMBUSTION MODELING	45
3.4.1	<i>SAGE model</i>	45
3.4.2	<i>FGM model</i>	47
3.5	EMISSION MODELING	48
3.5.1	<i>NO<sub>x</sub> modelling</i>	48
<b>4</b>	<b>COMBUSTION AND FLAME STABILITY</b>	<b>52</b>
4.1	COMBUSTOR DESIGN	53

4.1.1	<i>Combustor types</i>	54
4.1.2	<i>Diffuser</i>	56
4.2	COMBUSTION ZONES	57
4.2.1	<i>Primary zone</i>	58
4.2.2	<i>Intermediate zone</i>	59
4.2.3	<i>Dilution zone</i>	59
4.3	FUEL INJECTION	60
4.3.1	<i>Gas injection</i>	61
4.4	WALL COOLING	62
4.5	COMBUSTION FUNDAMENTALS	62
4.5.1	<i>Deflagration</i>	63
4.6	FLAME CLASSIFICATION	63
4.7	FLAMMABILITY LIMITS	64
4.8	FLAME STABILIZATION	65
4.8.1	<i>Measurement of stability performance</i>	66
4.8.2	<i>Bluff-Body Flameholders</i>	69
4.8.3	<i>Stability limits</i>	70
4.8.4	<i>Combustion chamber flame stabilization</i>	70
<b>5</b>	<b>MODEL CREATION AND CALIBRATION</b>	<b>73</b>
5.1	3D MODEL	73
5.2	CONVERGE DIAGNOSIS	79
5.3	BOUNDARIES DEFINITION AND CASE SETUP	81
5.3.1	<i>Materials</i>	84
5.3.2	<i>Simulation parameters</i>	84
5.3.3	<i>Physical Models</i>	85
5.3.4	<i>Grid control</i>	85
5.3.5	<i>Output/Post-processing</i>	85
5.4	EXPERIMENTAL DATA	86
5.5	RESULTS	89
<b>6</b>	<b>CONCLUSIONS AND FUTURE DIRECTIONS</b>	<b>104</b>
6.1	CONCLUSIONS	104
6.2	FUTURE DIRECTIONS	105
<b>7</b>	<b>TABLES INDEX</b>	<b>107</b>
<b>8</b>	<b>FIGURES INDEX</b>	<b>109</b>
<b>9</b>	<b>BIBLIOGRAPHY</b>	<b>113</b>



# **ABSTRACT**

*The continuous increase in worldwide energy request has made it necessary to study different ways to enhance the energy production efficiency. At the same time, the increase in global warming and the diffusion of ecological awareness campaigns have made sure to ratify a series of laws capable to ensure a decrease in pollutant emissions.*

*The purpose of this thesis is to perform Computational Fluid Dynamics (CFD) simulations for modelling an industrial gas turbine combustor in order to match the experimental pollutant emissions with the obtained results. To accomplish this task, a full scale 3D model of the combustor has been developed using the CAD software Pro/Engineer, eliminating some superfluous elements form the original geometry. As second step, the model has been imported in CONVERGE, an important and innovative CFD software which bypasses the mesh generation phase in order to decrease the total computational time. In CONVERGE two different combustion models, SAGE and FGM, have been developed and compared. To validate the models, the pollutant emissions of NO<sub>x</sub>, UHC and CO have been compared with the experimental results. It was found that the FGM model is the faster one in terms of computational time, and it also predicts the NO<sub>x</sub> and UHC pollutant emissions more precisely than the SAGE one.*

**Keywords:** *gas turbine, 3D model, combustion, combustion model, pollutant emission*



# 1 INTRODUCTION

Modern society consumes a large amount of fuel. For this reason, the energy industry is a fundamental part of the infrastructure of society in all countries. The energy industry is composed by the totality of companies involved in producing and selling energy. In particular, the gas turbines are and will be crucial in electrical energy generation industry.

The main tasks that must be accomplished by these turbines are high efficiency, low emissions and low costs. In order to satisfy the pollutant standards, is important to concentrate on the combustion system. For this reason, a technological combustor evolution and a detailed study of the combustion system is necessary to reach the imposed targets.

A complete analysis is developed thanks to the combination of numerical and experimental research. Experiments are at the same time expensive and time consuming. Moreover, during these experiments, the engine is not able to work properly.

These reasons, enforced by the continuous growing of computer technology, are enough to justify the diffusion of Computational Fluid Dynamics (CFD) analysis, used to perform simulations based on a defined numerical model. An optimal calibration of the model remains the main objective to respect as more as possible the reality.

## 1.1 PURPOSE OF THE STUDY

The objective of this project is to develop and calibrate a model able to simulate the behavior of an existing industrial gas turbine burner, in order to obtain precise pollutant predictions. Such model is developed using a high performance CFD software called CONVERGE, capable to handle complex geometries and to well simulate the chemistry of the combustion process.

All the main information about geometry, boundary conditions and experimental data are given by EthosEnergy S.p.a.

## **1.2 ETHOSENERGY S.P.A.**

EthosEnergy is an independent service provider of rotating equipment services and solutions to the power, oil & gas, and industrial markets. It has depth and experience in maintenance, asset operation, life cycle optimization & risk management. They are also specialized in power plant construction services.

EthosEnergy was born on May 6, 2014 thanks to an agreement between Siemens AG and John Wood Group PLC. The main objective of this joint venture was to merge the Siemens' TurboCare business unit and the Power and Maintenance Solutions businesses of the GTS division of Wood Group [1].

Recently, it has started a profitable collaboration with the DENERG department of the Italian university "Politecnico di Torino", in order to study from different points of view the FIAT TG20 B-7/8 gas turbine and to achieve higher efficiency and lower pollutant emissions on this engine.

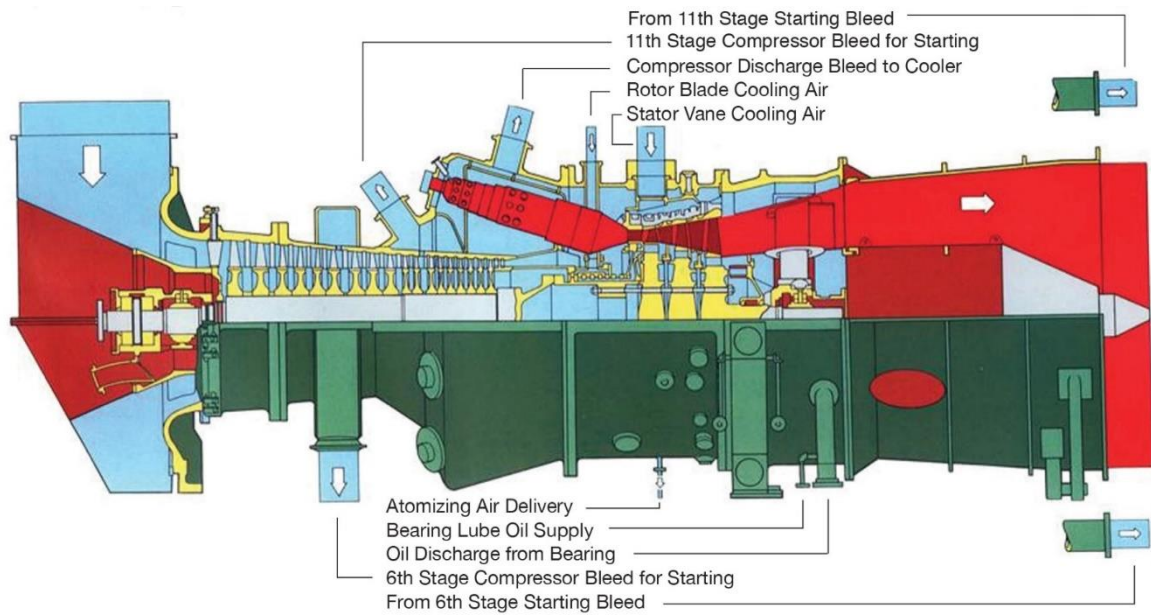


*Figure 1-1 Section view of FIAT TG20, courtesy of EthosEnergy*

### 1.3 GAS TURBINES

Combustion turbines, or better gas turbines, come from the family of the internal combustion engines. Gas turbine is a continuous combustion system characterized by three main elements:

- Compressor.
- Combustor.
- Turbine.

The first element is the rotating gas compressor, which absorbs the atmospheric air coming from the external environment. Inside the compressor the air pressure is increased. Then the air moves from the compressor to the combustor. Here fuel is injected, mixed with air and ignited, increasing the temperature and the pressure of the mixture and creating a continuous combustion. Then the high temperature and pressure exhaust gasses produced by the combustion go out from the combustor and enter inside the turbine. Here the exhausts expand and their pressure decrease,

producing a shaft work as output of the process. The shaft of the turbine is the same of the compressor. So, this shaft work can be used to drive the compressor. The energy that has not been used to compress the fluid, remains in the exhaust gasses, which can be used to produce an external work. In general, a gas turbine is connected to an additional power turbine, in which thrust is produced, and then it can be also transformed in electric energy thanks to the addition of an electrical generator. Then the air can be released in the external environment and the process can be repeated. This process is called Brayton cycle, and it is an open cycle, as previously described. The characteristics of this cycle are summarized in **Figure 1-3** and in **Figure 1-4**. In the **Figure 1-2** is presented an example of gas turbine structure.

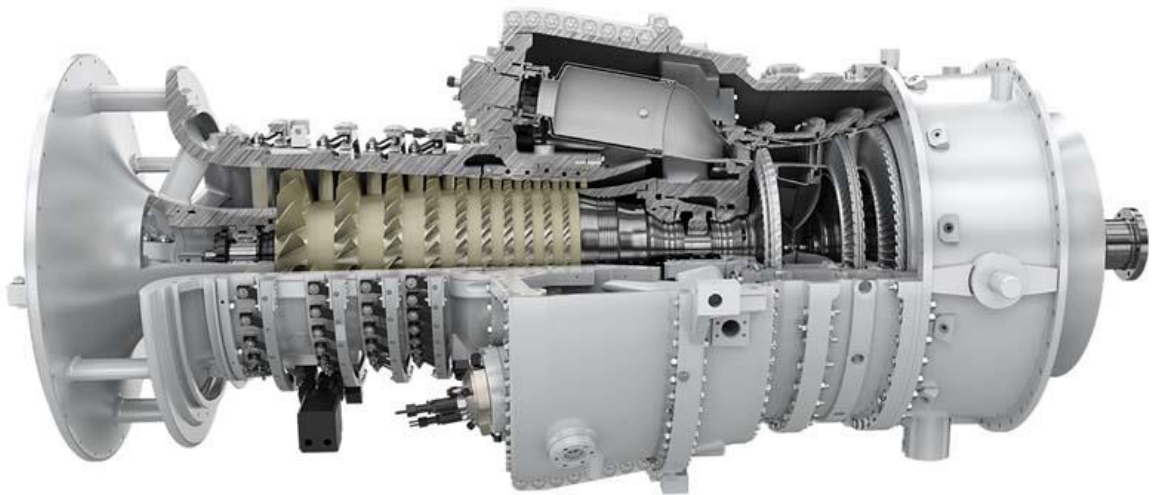


*Figure 1-2 A SGT-100 Siemens gas turbine [2].*

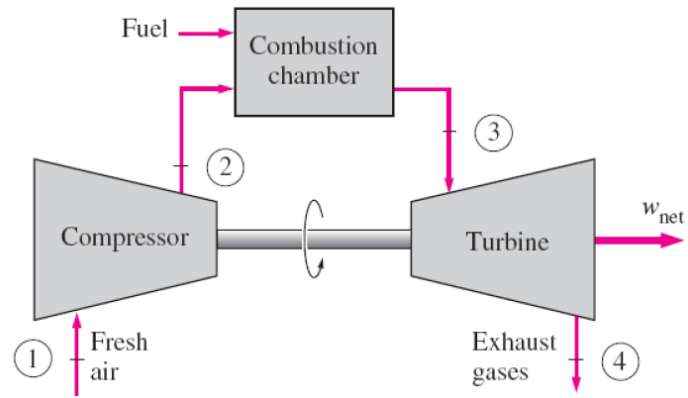


Figure 1-3 Schematic of the Brayton Cycle [3].

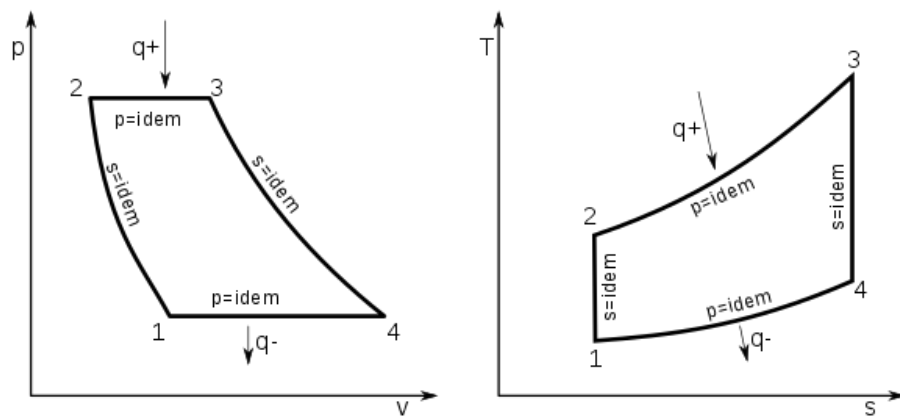


Figure 1-4  $p$ - $V$  and  $T$ - $s$  diagram for Brayton Cycle

## 1.4 THESIS OVERVIEW

This thesis work is divided into 6 chapters:

- In the following chapter, the first one, the scope of work is presented, and a brief introduction is reported.

- In the second chapter the theoretical background of the thesis is presented. It is fundamental to describe the interaction between combustion phenomena and turbulence, with the relative equations and simplifications. For this reason, all the equations describing the behavior of the reacting flow are reported. The main models for turbulence are also presented and discussed.
- The third chapter is based on the description of CONVERGE, the software used to develop the CFD analysis. All the main characteristics are presented, starting from solution methods until the mesh generation and grid size variation tools.
- The fourth chapter is based on the description of combustion phenomenon and flame stabilization. As first, the typical combustor designs are presented, in order to better understand the motivation behind each geometry. Then a brief description of the combustion zones and of the combustion fundamentals is performed. Finally, a very interesting argument has been faced: the flame stabilizations. Methods to study the flame stability are presented and characteristic of a stable flame are discussed.
- In the fifth chapter the effective thesis work is described. From the creation of the CAD model to the validation of the case setup and the starting of the simulations, all the steps are well described.
- Finally, in the last chapter an overview of the project is presented, together with the principal conclusions and future recommendations.



## 2 THEORETICAL BACKGROUND

A complete description of flames behavior is given by chemical composition and the transport equations of fluid. It is also possible to describe the fluid flow combining conservation equations for velocity, energy and mass.

Moreover, it is set out the chemical reacting part by the equations of state and by the mass evolution of each chemical species.

### 2.1.1 General continuity equations

The mass conservation can be described by the continuity equation

$$\frac{\partial \rho}{\partial t} + \nabla \cdot (\rho u) = 0, \quad (2.1)$$

where “t” is the time, u is the velocity vector and  $\rho$  is the density of the mixture.

The Navier-Stokes equation is used to describe the momentum conservation

$$\frac{\partial(\rho u)}{\partial t} + \nabla \cdot (\rho u u) + \nabla \cdot \tau + \nabla p - \rho g = 0. \quad (2.2)$$

Here, p represents the pressure, g is the gravitational acceleration and the stress tensor is represented by  $\tau$ .

Finally, it is also possible to describe the energy conservation. It can be done in terms of internal energy e or of specific enthalpy h.

In the described context, is better to use the enthalpy form, assuming the absence of volumetric heat source, because it is convenient in describing the reacting flow.

The equation is the following

$$\frac{\partial(\rho h)}{\partial t} + \nabla \cdot (\rho u h) + \nabla \cdot q + \tau : (\nabla u) - \frac{Dp}{Dt} = 0. \quad (2.3)$$

In this equation,  $q$  represents the heat flux, and  $h$  is the specific heat flux.

Is possible to notice that the enthalpy production due to pressure variation and viscous dissipation is represented by the last two terms of the equation.

Moreover, is possible to add another equation in order to describe the different composition of the reacting flow. The equation that is able to realize this task is the conservation of mass, written for all the chemical species.

$$\frac{\partial \rho_i}{\partial t} + \nabla \cdot (\rho_i u_i) = \dot{\omega}_i \quad i \in [1, N_s], \quad (2.4)$$

where  $N_s$  is the total amount of species,  $\rho_i$ ,  $u_i$  and  $\omega_i$  are respectively density, three-dimensional velocity vector and chemical source term of the  $i$  species.

The destruction or creation of the species, which is represented by  $\omega_i$ , is directly connected to a chemical reaction mechanism. However, this mechanism is not able to change the total amount of mass.

This means that each  $i$  term of the equation can be summed, obtaining at the end the complete transport equation.

So

$$\sum_{i=1}^{N_s} \dot{\omega}_i = 0 \quad (2.5)$$

The conservation of mass for all the species can be also written in the following way

$$\frac{\partial \rho Y_i}{\partial t} + \nabla \cdot (\rho Y_i u) = -\nabla \cdot (\rho Y_i U_i) + \dot{\omega}_i \quad i \in [1, N_s], \quad (2.6)$$

where

$$u_i = u + U_i, \quad (2.7)$$

$$Y_i = \frac{\rho_i}{\rho}. \quad (2.8)$$

Here,  $U_i$  represents the diffusion velocity, which is the deviation velocity of the species  $i$  respect on the bulk flow velocity  $u$ .  $Y_i$  is the species mass fraction.

This formulation is important in order to divide the different physical contributions that can be identified inside the equation. The first term represent the time-dependency, the second is connected to the convection, the third to the diffusion and the last one represent the chemical production [4]. So is possible to change the 2.5 in the following formulation, highlighting that also the sum of the diffusion velocities goes to zero:

$$\sum_{i=1}^{N_s} Y_i \dot{\omega}_i = 0 \quad (2.9)$$

### 2.1.2 Thermal and caloric equation of state

The thermal equation is able to connect pressure to different parameters, such as density, species mass fractions and temperature [4]. In this system of equations, these three parameters are primitive variables. All the species present in the flow behaves like an ideal gas.

The ideal gas law, evaluated for partial pressure, is

$$p_i = n_i R^0 T, \quad (2.10)$$

where  $R^0$  is the gas constant,  $n_i$  is the molar concentration of the  $i$  species and  $T$  is the temperature of the mixture.

Knowing that

$$n_i = n \cdot X_i = \rho \frac{Y_i}{M_i}, \quad (2.11)$$

where  $n$  is the total molar concentration,  $X_i$  is the species mole fraction and  $M_i$  is the molecular mass of the  $i$  species, is possible to write the total pressure as

$$p = \sum_{i=1}^{N_s} p_i = \sum_{i=1}^{N_s} \rho R^0 T \frac{Y_i}{M_i}. \quad (2.12)$$

Thanks to the caloric equation of state, it is possible to evaluate the species enthalpy

$$h_i = h^{ref} + \int_{T^{ref}}^T c_{p,i} T dT, \quad (2.13)$$

where  $h^{ref}$  and  $T^{ref}$  are respectively reference enthalpy and temperature, and  $c_{p,i}$  is the specific heat at constant pressure of the species  $i$ . Also, in this case, is possible to sum all the  $h_i$  contribution to obtain the total enthalpy of the mixture

$$h = \sum_{i=1}^{N_s} h_i. \quad (2.14)$$

### 2.1.3 Transport Models

It is possible to use the Stokes' law of friction, in order to model the viscous stress tensor

$$\tau = \mu(\nabla u + (\nabla u)^T) - \frac{2}{3} (\nabla \cdot u) I, \quad (2.15)$$

where  $I$  is the unit tensor and  $\mu$  represents the dynamic viscosity of the mixture. Referring on the equation 2.6, it is possible to derive the diffusion velocity field thanks to the Stefan-Maxwell equations, neglecting the effect of temperature and pressure gradients on diffusion velocity

$$\nabla X_i = \sum_{j=1}^{N_s} \frac{X_i X_j}{D_{ij}} (U_j - U_i). \quad (2.16)$$

Here  $D_{ij}$  is binary mass diffusion coefficient of species  $i$  into species  $j$ . Is necessary to simplify the previous equation using the Fick's Law, because otherwise the computation results to be too expensive.

The Fick's Law reads

$$U_i = -\frac{D_i}{X_i} \nabla X_i, \quad (2.17)$$

with  $D_i$  that in this case is representing mixture-averaged diffusion coefficient.

Moreover, Fourier's law can be used to evaluate the heat flux vector

$$q = -\lambda \nabla T + \rho \sum_{i=1}^{N_s} h_i U_i Y_i, \quad (2.18)$$

where  $\lambda$  represents the thermal conductivity of the mixture. It is possible to distinguish two different contributions, the first one due to conduction, the second one due to mass diffusion. Using the equations 2.13 and 2.17 it is possible to write the Fourier's Law in the following equation

$$q = -\frac{\lambda}{c_p} \nabla h + \frac{\lambda}{c_p} \sum_{i=1}^{N_s} h_i \nabla Y_i \left( \frac{1}{Le_i} - 1 \right), \quad (2.19)$$

where  $Le_i$  is the dimensionless Lewis number, that represents the ratio of thermal conduction and mass diffusivity of the species.

$$Le_i = \frac{\lambda}{c_p D \rho}, \quad (2.20)$$

where  $\frac{\lambda}{c_p}$  is the thermal diffusivity and  $D \rho$  is the mass diffusivity. This means that if the Lewis number is different from one, the two contributions are not characterized by the same rate in the flame, so species and heat locally redistribute.

In case of fuels such as methane, in the turbulent combustion models is a valid assumption to consider  $Le_i = const.$  [4]

To model the dynamic viscosity, are used the following equations

$$\mu = \sum_{i=1}^{N_s} \frac{Y_i \mu_i}{M_i \left( \sum_{j=1}^{N_s} \frac{Y_j \Phi_{ij}}{M_{ij}} \right)}, \quad (2.21)$$

$$\Phi_{ij} = \frac{1}{\sqrt{8}} \left( 1 + \frac{M_i}{M_j} \right)^{-\frac{1}{2}} \left[ 1 + \left( \frac{\mu_i}{\mu_j} \right)^{\frac{1}{2}} \left( \frac{M_i}{M_j} \right)^{\frac{1}{4}} \right]. \quad (2.22)$$

Finally, the expressions for the thermal conduction and mass diffusivity are shown:

$$\lambda = \frac{1}{2} \left[ M \sum_{i=1}^{N_s} \frac{Y_i \lambda_i}{M_i} + \left( M \sum_{i=1}^{N_s} \frac{Y_i}{M_i \lambda_i} \right)^{-1} \right], \quad (2.23)$$

$$D_i = \frac{1 - Y_i}{M \sum_{j \neq i}^{N_s} \frac{Y_j}{M_j D_{ij}}}. \quad (2.24)$$

The dependence on pressure and temperature gradient has been neglected in order to reduce the computational time cost of the CFD analysis [4].

As final step, the equation 2.19 can be added to the conservation equations for enthalpy and species, obtaining

$$\frac{\partial(\rho h)}{\partial t} + \nabla \cdot (\rho u h) = \nabla \cdot \left( \frac{\lambda}{c_p} \nabla h \right) + \nabla \cdot \left[ \frac{\lambda}{c_p} \sum_{i=1}^{N_s} h_i \nabla Y_i \left( \frac{1}{Le_i} - 1 \right) \right] + \rho u g + \tau : (\nabla u) + \frac{Dp}{Dt}, \quad (2.25)$$

$$\frac{\partial \rho Y_i}{\partial t} + \nabla \cdot (\rho Y_i u) = \nabla \cdot \left( \frac{\lambda}{Le_i c_p} \nabla Y_i \right) + \dot{\omega}_i. \quad (2.26)$$

## 2.2 COMBUSTION CHEMISTRY

Combustion is a chemical reaction based on the presence of reactants and products. The reactant is the fuel, methane in this project. This reaction is exothermic and is composed by a sequence of chemical reactions. It is not so easy to give a complete overview of these reactions, so is preferred to show the first and the last step of the combustion, avoiding all the intermediate passages. The global reaction of combustion of methane with air is the following:



however, is possible to represent the general elementary reactions using the expression:

$$\sum_{i=1}^{N_R} v'_{ij} A_i \rightleftharpoons \sum_{i=1}^{N_R} v''_{ij} A_i, \quad (2.28)$$

where  $v'_{ij}$  and  $v''_{ij}$  represent the forward and backward molar stoichiometric coefficients of species  $i$  and reaction  $j$ , while  $A_i$  represent species  $i$  and  $N_R$  is the total number of reactions.

Is possible to use the molar stoichiometric coefficients in order to describe  $\omega_i$ , the chemical source term of species  $i$ .

$$\dot{\omega}_i = M \sum_{i=1}^{N_R} (v''_{ij} - v'_{ij}) r_j, \quad (2.29)$$

with  $r_j$  the reaction rate for elementary reaction  $j$ .

## 2.3 TURBULENCE MODELING

The continuity, thermal and caloric equations, together with the transport model, described previously, are useful to define completely the turbulent fluid flow. DNS, or Direct Numerical Solution, is the name of the plain solution of this system of equations. Is possible to estimate the computational time to solve the turbulence, thanks to the proportionality between the number of CPU operations, the number of mesh points and finally the one of time steps. The final computational time for DNS results to be too high, so his usage results to be limited to small scale academic

problems. To reduce the computational time and solve large scale and complex problems, is fundamental to use models.

Two widely used approaches are LES and RANS.

The first one is the Large Eddy Simulation approach. It is able to reduce the time cost of the simulation by low-pass filtering the small scales. The final solution is a filtered velocity field. Is also necessary to include a model able to represent of the small-scale motion and its influence (sub-grid). So, LES is able to solve the largest scales of turbulence and model the rest by use of sub-grid turbulence models or by blending with a RANS model.

Anyways, despite all the techniques used to decrease the computational time, still it is not enough. For this reason, the RANS approach has been used for this project.

Reynolds Averaged Navier-Stokes (RANS) model attempt to close the turbulence equations using viscosity terms. A common variable calculated in these models is  $k$ , or the kinetic energy per unit mass of turbulent fluctuations. The solution is a mean velocity field, and models are useful to represent fluctuations of the flow that are not solved [4].

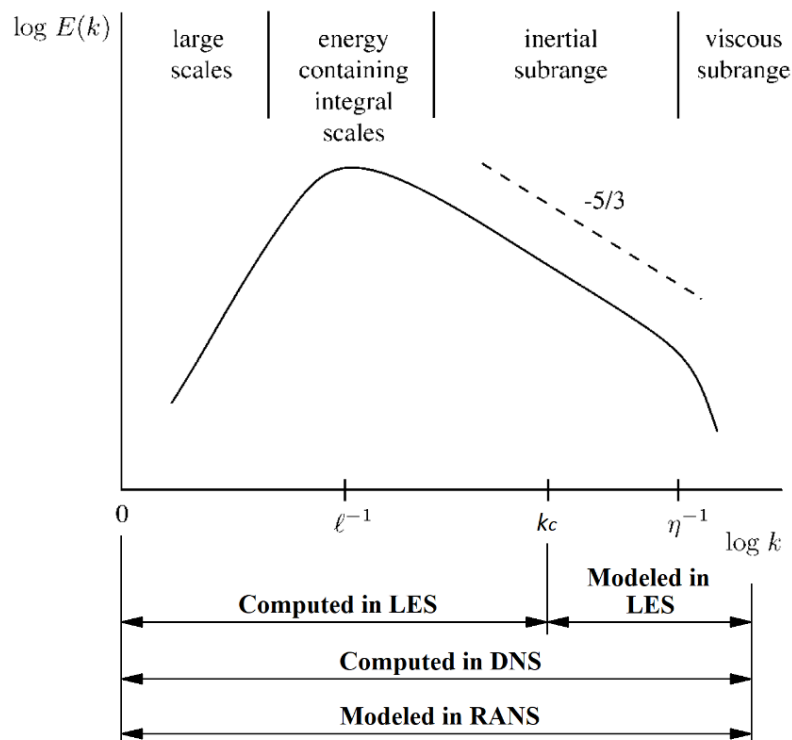


Figure 2-1 Turbulent kinetic energy spectrum

### 2.3.1 Reynolds-Averaged Navier-Stokes (RANS) Equations

RANS model is characterized by an acceptable results simplification and a lower computational time. For these reasons, it is used for most of engineering applications.

In Reynolds-Averaged approaches, the unsteadiness is averaged out i.e. them all are considered as part of the turbulence. This modification is obtained by describing the instantaneous flow quantities as the sum of two different terms: the first one represents the mean value and the second one is a time-dependent fluctuating value, about the mean one. The equation is the following

$$u(x, t) = \bar{u}(x) + u'(x, t), \quad (2.30)$$

where the mean velocity can be written as

$$\bar{u}(x) = \lim_{T \rightarrow \infty} \frac{1}{T} \int_0^T u(x, t) dt. \quad (2.31)$$

Here T is the averaged time, that should be large enough, in order to eliminate the dependence of  $\bar{u}(x)$  on the time at which the time is averaged. It can be used only if the flow is steady, otherwise it should be substituted by the following formulation:

$$\bar{u}(x, t) = \lim_{N \rightarrow \infty} \frac{1}{N} \sum_{n=1}^N u(x, t), \quad (2.32)$$

where N, the total number of members in the summation, should be large enough in order to eliminate the fluctuation effects. This Reynolds-Averaged approach is

applied to the Navier-Stokes equations, in order to obtain the Reynolds-averaged Navier-Stokes (RANS) ones. The time average of the fluctuating part results to be zero, while the average of the mean part remains the same. Thus, if any linear term in the conservation equations is averaged, results in the identical term for the averaged quantity

If we consider a quadratic nonlinear term, it results in two terms

$$\overline{u_i u_j} = \overline{(\bar{u}_i + u'_i)(\bar{u}_j + u'_j)} = \bar{u}_i \bar{u}_j + \overline{u'_i u'_j}. \quad (2.33)$$

The first term is the product of the two averages, the second one is the covariance, that can be zero only if the two quantities of the product are not correlated. In general, for turbulent flow, they are correlated, so is possible to notice in the conservation equation some terms called Reynolds Stresses. These terms are typically written as  $\rho \overline{u'_i u'_j}$ . There are also other terms, like  $\rho \overline{u'_i \phi'}$ , known as turbulent scalar fluxes, which, together with the Reynolds Stresses, indicate that the latter is not closed, so the number of variables is higher than the one of the equations.

In order to solve the system of equations, is important to simplify these terms. Generally, they are evaluated as mean quantities. The approximations that have been introduced are defined as “turbulence models”. If is considered an incompressible flow without body forces, is possible to write the Reynolds averaged equations of motion, in conservation form

$$\frac{\partial(\rho \bar{u}_i)}{\partial x_i} = 0, \quad (2.34)$$

$$\frac{\partial(\rho \bar{u}_i)}{\partial t} + \frac{\partial}{\partial x_j} (\rho \bar{u}_i \bar{u}_j + \rho \overline{u'_i u'_j}) = -\frac{\partial \bar{p}}{\partial x_i} + \frac{\partial \bar{\tau}_{ij}}{\partial x_j}, \quad (2.35)$$

$$\bar{\tau}_{ij} = \mu \left( \frac{\partial \bar{u}_i}{\partial x_j} + \frac{\partial \bar{u}_j}{\partial x_i} \right). \quad (2.36)$$

Here the term  $\bar{\tau}_{ij}$  represents all the components of the mean viscous stress tensor.

### 2.3.2 Turbulence Models

Four different kind of turbulence models have been developed:

- Algebraic (Zero-Equation) Models (e.g. eddy-viscosity/mixing-length, etc.).
- One-Equation Models like Bradshaw-Ferriss-Atwell model, Allmaras and Spalart model, etc. They are widely used because of their simplicity respect on the other models. In fact, they can be solved easier numerically.
- Two-Equation Models: k- $\omega$  model, k- $\epsilon$  model, and their modified versions.
- Second-Order Closure Models like Rodi, Reece and Launder model, etc. This last family is characterized by an increase in complexity because of the larger number of equations, so is used in a limited number of applications respects on the One-Equation and Two-Equation Models.

Actually, the One-Equation and Two-Equation Models are the most used ones. They both are characterized by the Boussinesq eddy-viscosity approximation, but there is a fundamental difference between these two models. The first family relates the turbulence length scale to some typical flow dimension so, for this reason, it is incomplete. The Two-Equation Models are able to define a formulation for the turbulence length scale. Moreover, the second family gives also the possibility to detect the kinetic energy per unit length (k). For all these reasons, it is defined as complete.

### 2.3.3 RNG k- $\epsilon$ Turbulence Model

RANS models are able to model the Reynolds stress term through an effective turbulent viscosity. This simplification is justified by the fact that in laminar flows,

transport of energy, momentum and mass, and the energy dissipation are averaged by the viscosity. Consequently, is acceptable to represent the effect of turbulence as an increase in viscosity [5].

$$-\rho \overline{u'_i u'_j} = \mu_t \left( \frac{\partial \bar{u}_i}{\partial x_j} + \frac{\partial \bar{u}_j}{\partial x_i} \right) - \frac{2}{3} \rho \sigma_{ij} k, \quad (2.37)$$

$$k = \frac{1}{2} \overline{u'_i u'_i} = \frac{1}{2} (\overline{u'_x u'_x} + \overline{u'_y u'_y} + \overline{u'_z u'_z}), \quad (2.38)$$

$$\mu_t = \rho C_\mu \sqrt{k} L = \rho C_\mu \frac{k^2}{\varepsilon}. \quad (2.39)$$

Here  $\sigma_{ij}$  is the stress tensor,  $\mu_t$  represents the turbulent eddy viscosity,  $k$  is the turbulent kinetic energy,  $C_\mu$  is a model constant that can be tuned for a particular flow,  $L$  is the turbulence length scale and finally  $\varepsilon$  represents the dissipation term of the turbulent kinetic energy.

The turbulence kinetic energy equation can be written in the following way:

$$\frac{\partial(\rho k)}{\partial t} + \frac{\partial(\rho \bar{u}_j k)}{\partial x_j} = \frac{\partial}{\partial x_j} \left( \mu \frac{\partial k}{\partial x_j} \right) - \frac{\partial}{\partial x_j} \left( \frac{\rho}{2} \overline{u'_j u'_i u'_i} + \overline{p' u'_j} \right) - \rho \overline{u'_i u'_j} \frac{\partial \bar{u}_i}{\partial x_j} - \mu \frac{\partial \bar{u}_i}{\partial x_k} \frac{\partial \bar{u}_i}{\partial x_k}, \quad (2.40)$$

It is necessary to model only the last three terms of the right-hand side. In particular, the second term represents the turbulent diffusion of kinetic energy, the third one represents the production rate of turbulent kinetic energy multiplied by the mean flow, so it represents a kinetic energy transfer, which comes from the mean flow and goes to the turbulence. Finally, the last term is the product between the dissipation  $\varepsilon$  and density, which describes the conversion rate of turbulence energy in internal energy. This rate is irreversible.

The primary objective for the formulation of the  $k$ - $\varepsilon$  model is to define an exact equation for the dissipation  $\varepsilon$  and then to find a good approximation for the equation that is governing its behavior.

An exact equation for  $\varepsilon$  can be computed from the Navier-Stokes equations, obtaining the following formulation:

$$\frac{\partial(\rho\varepsilon)}{\partial t} + \frac{\partial(\rho u_j \varepsilon)}{\partial x_j} = \frac{\partial}{\partial x_j} \left( \frac{\mu + \mu_t}{Pr_\varepsilon} \frac{\partial \varepsilon}{\partial x_j} \right) + C_{\varepsilon 3} \rho \varepsilon \frac{\partial u_i}{\partial x_i} + \frac{\varepsilon}{k} \left( C_{\varepsilon 1} \frac{\partial u_i}{\partial x_i} \tau_{ij} - C_{\varepsilon 2} \rho \varepsilon \right) - \rho R, \quad (2.41)$$

Where  $Pr_\varepsilon$  is the reciprocal  $\varepsilon$  Prandtl number,  $\mu$  is the molecular viscosity and  $C_{\varepsilon 1}$ ,  $C_{\varepsilon 2}$ ,  $C_{\varepsilon 3}$  are the model constants. These constants are characterized by a certain value connected to the engineering application. The last term of the equation,  $\rho R$ , defines the difference between standard k- $\varepsilon$  and RNG k- $\varepsilon$  models. If this term is present, the RNG k- $\varepsilon$  model is used, otherwise is used the standard one.  $R$  can be written as:

$$R = \frac{C_\mu \eta^3 \left(1 - \frac{\eta}{\eta_0}\right) \varepsilon^2}{1 + \beta \eta^3} \frac{1}{k}, \quad (2.42)$$

$$\eta = \frac{k}{\varepsilon} \sqrt{2 S_{ij} S_{ij}}, \quad (2.43)$$

$$S_{ij} = \frac{1}{2} \left( \frac{\partial \bar{u}_i}{\partial x_j} + \frac{\partial \bar{u}_j}{\partial x_i} \right), \quad (2.44)$$

$$\eta_0 = \left[ \frac{C_{\varepsilon 2} - 1}{C_\mu (C_{\varepsilon 1} - 1)} \right]^{\frac{1}{2}}, \quad (2.45)$$

where  $\beta$  is a constant.

The RNG model is based on the renormalization of Navier-Stokes equations through the Re-Normalization Group (RNG) methods. In particular, evaluating the eddy viscosity, the RNG k- $\varepsilon$  model is able to define different turbulence length scales, instead of considering only one, as in the standard model. This difference is fundamental in order to define all the contributions of the turbulence dissipation, being influenced by all the scales

It is presented a table which contains the values for the previously cited constants:

Constant	Value
$C_{\varepsilon 1}$	1.42
$C_{\varepsilon 2}$	1.68
$C_{\varepsilon 3}$	-1.0
$Pr_{\varepsilon}$	1.39
$C_{\mu}$	0.0845
$\eta_0$	4.38
$\beta$	0.012

*Table 2-1 RNG k- $\varepsilon$  constants and relative value*



### 3 CONVERGE CFD Tool

CONVERGE is a revolutionary CFD software. It is characterized by the capability to create an autonomous mesh. This autonomous mesh can evolve dynamically in time and space and uses the AMR (Adaptive Mesh Refinement) tool in order to maximize computational efficiency and accuracy. Thanks to this important task, it is able to simplify and to speed up the simulation process eliminating the grid generation bottleneck. It is a product of Convergent Science, which is an innovative computational fluid dynamics (CFD) company. It has been founded in 1997 by a group of graduated students and it is headquartered in Madison, Wisconsin [6].

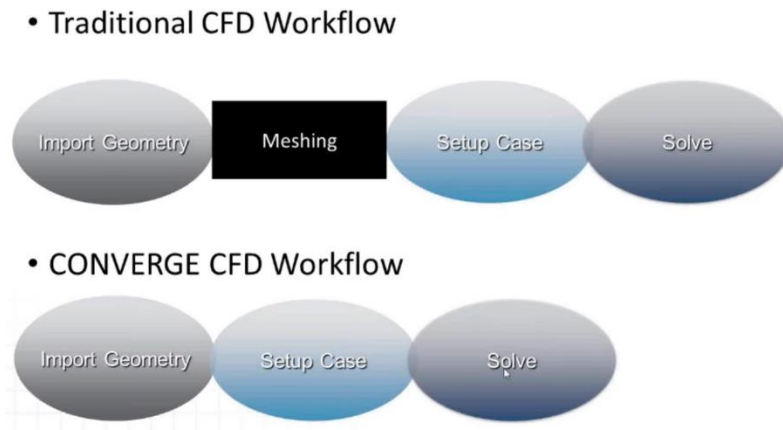


**Figure 3-1** Comparison between the traditional CFD and CONVERGE workflow [6].

### 3.1.1 Discretization methods

Any numerical method is characterized by a set of integro-differential or partial differential equations plus a certain number of boundary conditions, which represents the mathematical model. Then in order to approximate the differential equations, is fundamental to choose an appropriate discretization method. It is used to reduce the governing partial differential equations to a set of algebraic equations. Many approaches can be used to perform the discretization, but the most important and diffused ones are Finite Volume (FV), Finite Difference (FD), and Finite Element (FE) methods.

In particular, the Finite Volume method is a commonly used in CFD codes, thanks to its advantage in solution speed and memory usage respect on the other methods. In FV method, the governing partial differential equations are written in a conservative form, and then solved over discrete control volumes. In particular, the domain is subdivided into a certain number of contiguous control volumes. On each CV the conservation equations are imposed. The variable values are computed on a node in the center of each control volume and, in order to transform variable values at the control volume surface as nodal values, interpolation is performed. Moreover, this method is used also for large and complex geometries and it guarantees the conservation of energy, mass and momentum.

The integral form of the equation can be solved performing a summation of all the fluxes on the faces of the cells, but the variable values are stored in the middle of each cell or control volume. This means that the values have to be interpolated to the surface of the cells. An example is provided by the **Figure 3-2**.

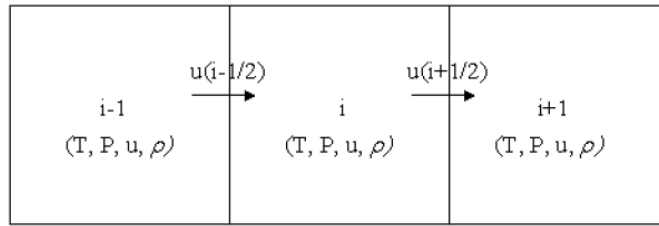


**Figure 3-2** Sample three-cell, one-dimensional spatial domain [5].

To perform this task, there are different methods, e.g. is possible to average two adjacent cell values and then put them on the surface [5]

$$\phi_{i\pm\frac{1}{2}} = \frac{1}{2}\phi_i + \frac{1}{2}\phi_{i\pm 1}. \quad (3.1)$$

### 3.1.2 Solution procedure

It is fundamental to understand the scheme followed by CONVERGE in order to solve the transport equations. In **Figure 3-3** is presented the resolution order.

The previous values for all transported quantities are stored at the start of each time-step. Then, it is possible to calculate explicit sources for each sub-model activated and finally, if energy and radiation are decoupled, radiation is solved. At the first PISO iteration, CONVERGE have to solve the equations for momentum and pressure. In this way, it is able to set the velocity for the other transport equations. For each PISO iteration, PISO loop convergence must be checked. For compressible cases, PISO loop converges if [5]:

$$\Delta\rho < \textit{piso\_tol}, \quad (3.2)$$

Here  $\Delta\rho$  is the density correction error and *piso\_tol* represents the PISO tolerance.

For incompressible cases, PISO loop converges if:

$$\Delta P < \textit{piso\_tol}, \quad (3.3)$$

where  $\Delta P$  represents the pressure correction error. If the PISO iteration did not converge, CONVERGE executes an additional PISO iteration.

After the PISO loop has ended, an additional Jacobi iteration can be performed by Converge, in order to enforce strict conservation. Depending on the inputs, CONVERGE can perform this iteration in a different way. The Jacobi iteration is able to guarantee the conservation of the quantity to machine zero, rather than to the piso tolerance [5].

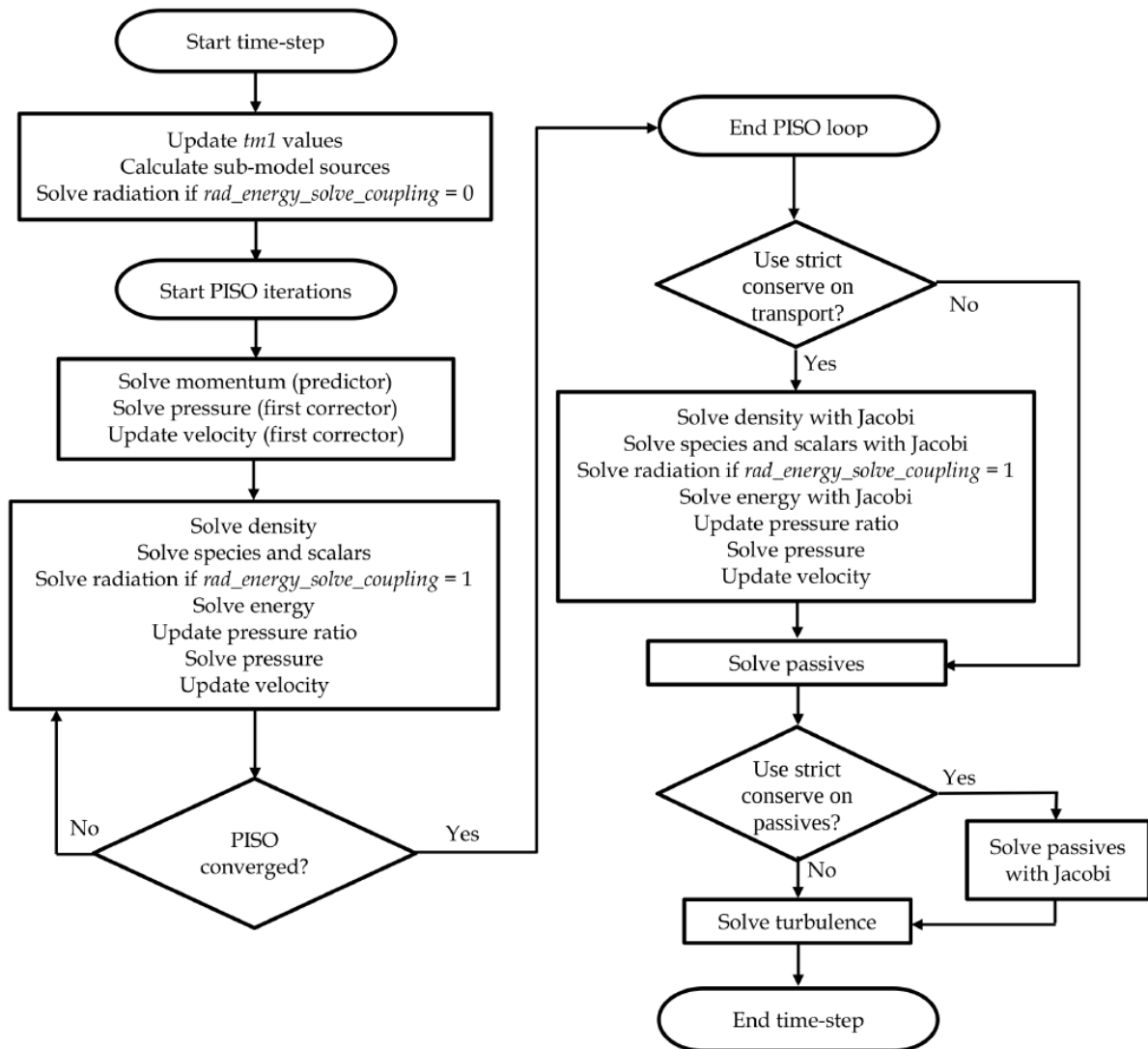


Figure 3-3 CONVERGE solution procedure [5].

### 3.1.3 PISO algorithm

CONVERGE achieves the pressure-velocity coupling using the PISO method. The CONVERGE PISO algorithm starts with a predictor step, evaluated where the momentum equation is solved. After, it is possible to derive and solve a pressure equation, which permits to derive and apply a correction to the momentum equation. This process can be repeated as many times as necessary in order to achieve the desired momentum equation accuracy. It is possible to define a minimum and maximum number of PISO iterations. If the maximum number is exceeded without reaching the convergence, the following time-step will be reduced. After these initial

steps have been completed, CONVERGE is able to solve all the other transport equations in series [5].

The PISO method has been chosen to be used in CONVERGE for many reasons. With only minor variations, it can be used for compressible or incompressible flow problems. Moreover, the predictor-corrector concept gives the possibility to perform a semi-implicit treatment for sources and sinks: they can be updated continuously. PISO respects the transport equations hyperbolic nature, while using the pressure equation elliptic nature to make faster the diffusion of information through the domain. A detailed explanation of PISO algorithm can be found in [5]

### 3.1.4 CFL number

The Courant–Friedrichs–Lewy (CFL) numbers are able to estimate the number of cells through which the related quantity will move in a single time-step. Generally, a higher CFL number corresponds to a lower computational time for the simulation. The convective, speed of sound and diffusive CFL numbers are respectively [5]:

$$cfl_u = u \frac{\Delta t}{\Delta x}, \quad (3.4)$$

$$cfl_{mach} = c \frac{\Delta t}{\Delta x}, \quad (3.5)$$

$$cfl_v = v \frac{\Delta t}{\Delta x^2}. \quad (3.6)$$

Here  $\Delta x$  is the grid scaling,  $\Delta t$  represents the time step. The viscosity, the speed of sound and the cell velocity are represented respectively by  $\nu$ ,  $c$  and  $u$ .

### 3.1.5 Steady-state solver

CONVERGE gives the possibility to use the steady-state solver, which guarantees faster solutions to steady-state problems where transient behavior is not needed. Steady-state problems can be solved using the transient solver, but this method is not efficient and consequently not recommended [5].

It is possible to write the transport equation for steady state conditions:

$$\nabla \cdot (\rho Y_i u) = \nabla \cdot \left( \frac{\lambda}{Le_i c_p} \nabla Y_i \right) + \dot{\omega}_i. \quad (3.7)$$

The previous formulation is time independent. For this reason, in CONVERGE is introduced a so-called pseudo-time, which is useful to solve the **equation 3.7**.

The rate of convergence is improved if compared with the transient solver, because the steady-state solver does not have to be time-accurate while proceeding in pseudo time. The maximum convection CFL number defines the pseudo time-step size for each cycle. The larger the convection CFL number the lower the number of cycles required to reach a steady-state value [5].

## 3.2 BOUNDARY CONDITIONS

A boundary condition represents a stated restriction, usually in the form of an equation, able to limit the possible solution to a differential equation. For this reason, in order to simplify the resolution of the previously discussed system of equations, it is necessary to define a certain number of boundary conditions. This number is connected to the highest order derivative in each independent variable.

There are different types of boundaries which can be set in CONVERGE: inflow, outflow, wall, symmetry, periodic, two\_d, gt-suite or interface. It is also needed to define a boundary condition at each boundary for each partial differential conservation equation [5]. They can be respectively Dirichlet or Neumann:

$$\Phi = f, \quad (3.8)$$

$$\frac{\partial \Phi}{\partial x} = f, \quad (3.9)$$

where  $\Phi$  is a general solved quantity (e.g. energy, pressure, species, or velocity) and  $f$  represents the specified value or derivative on the boundary. In CONVERGE,  $f$  is generally set to zero [5].

The boundaries set in CONVERGE for this project are of the type inflow, outflow and wall.

Outflow and inflow boundaries are very similar, but there are some important differences in options available and boundary conditions. For example, in outflow boundaries, it is necessary to set boundary conditions for backflow, which is the amount of flow entering from the outflow boundary. An incorrect setting of these BCs can seriously influence the convergence of the solution. Certain combinations of boundary conditions are not be stable and must be avoided. For example, an outflow Neumann pressure boundary condition and an inflow Neumann pressure boundary condition can result in the mean domain pressure drifting [5].

Wall boundaries in CONVERGE can be moving or fixed. In the first case the BCs are applied to a surface which moves, in the second one the surface is fixed. Thanks to this boundary, it is possible to define on the entire surface the value of different parameters like velocity, pressure, temperature, turbulent kinetic energy, turbulent dissipation and specific dissipation rate. It is also possible to set information about passives and species [5].

### 3.3 MESH GENERATION

CONVERGE automatically generates an orthogonal grid at runtime based on a few user-defined grid control parameters, dynamically adapts the mesh throughout the simulation, and invokes Adaptive Mesh Refinement to maximize both accuracy and computational efficiency. To perform this task, CONVERGE applies a cut-cell Cartesian method, in order to generate the grid.

The geometry surface is inside a Cartesian block. CONVERGE is able to cut the cells at the intersection, then the intersection information, like normal vectors or surface areas, is reduced and finally it is stored for each cell. This permits represented more easily complex surface intersections [5].

In particular, if CONVERGE finds a cut-cell with a volume which is less than 30% of the adjacent cell, the two cells are paired together, in order to create a single node. This process is called cell pairing. The new center of the cell is positioned in its volumetric center. Moreover, the transport entities values, like pressure, temperature and velocity, are shared by the cut-cell and the regular one [5]. In the **Figure 3-4** is reported an example of cut-cell and in the **Figure 3-5** is presented an example of cell-pairing.

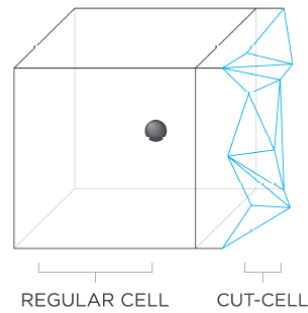


**Figure 3-4** A regular cell combined with a cut-cell [5]

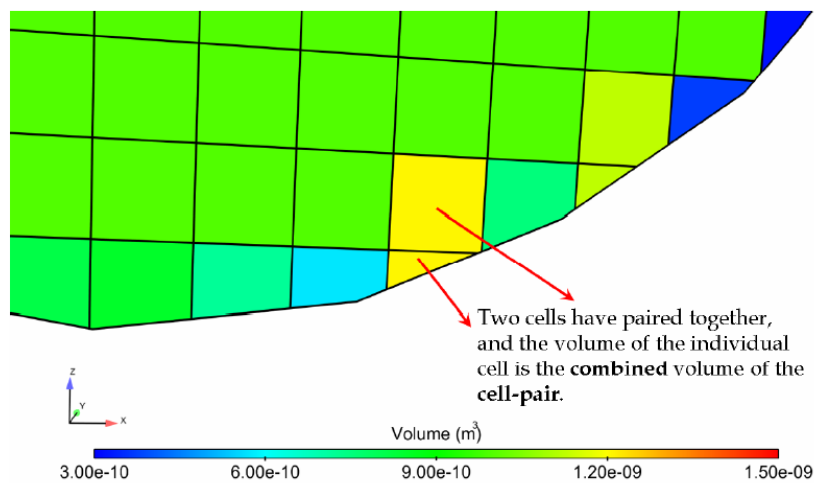


**Figure 3-5** Cell Pairing [5]

The grid generation follows a specific process:

- the surface is moved to the proper location;
- the boundary cells are trimmed;
- embedding areas are refined;
- refinement from the embedding are removed.

If it is working with stationary geometries, as in the studied case, CONVERGE repeats this process two times: when the simulation starts and after the refinement (or coarsening).

### 3.3.1 Grid scaling

Grid scaling defines the change in base grid size in specific moments during a simulation. It is able to reduce the simulation runtime during non-critical simulation steps by coarsening the grid. Moreover, it can refining the grid at other times, helping in capture critical flow phenomena [5].

This change in base grid size is based on the following formulation:

$$ds_{scaled} = \frac{ds_{base}}{2^{grid\_scale}}, \quad (3.10)$$

where *grid\_scale* represents the scaling factor, and *ds\_scaled* is the spatial coordinate that is obtained from the *ds\_base*, thanks to the scaling factor. If the grid scale value is zero, the grid size is unchanged. In order to refine the base grid, is used a positive value. In opposition, to coarse it, a negative value is necessary.

### 3.3.2 Fixed embedding

Fixed embedding is a fundamental tool used in order to refine locally the grid where a finer resolution is needed to reach a higher accuracy of the solution. Thanks to the local refinements, it allows to remain coarse the rest of the grid, and this permits to minimize simulation time [5].

The embedding scaling is based on the following equation:

$$ds_{embed} = \frac{ds_{base}}{2^{embed\_scale}}, \quad (3.11)$$

where *embed\_scale* indicated how much a certain location must be scaled by CONVERGE. In this case, its value can be only positive, because the objective is to refine the mesh in a specific location. In order to reduce the computational time, it is also possible to apply the embedding scaling in a specific time period.

It is possible to distinguish different kind of fixed embedding:

- Boundary embedding: is used to provide a finer grid near a boundary;
- Sphere embedding: is used to embed a spherical area, defined by its center and radius;
- Cylindrical embedding: is used to embed a cylindrical or truncated conical area;
- Region embedding: is used to provide a finer grid in an entire region;
- Box embedding: is used to embed a generic “box” area;
- Nozzle and injector embedding: is used to embed the conical area around the nozzle or the one around all the nozzles of an injector.

In the following figures are reported some examples of embedding:

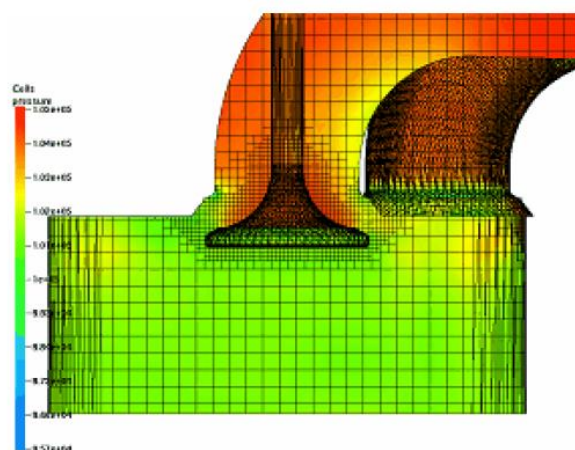


**Figure 3-6** A visualization of Boundary embedding around a valve [5]

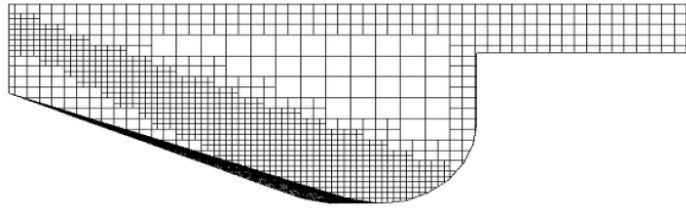


*Figure 3-7 A grid generated using nozzle embedding [5]*

### 3.3.3 Adaptive mesh refinement (AMR)

Adaptive Mesh Refinement (AMR) is used to refine automatically the grid through moving and fluctuating conditions like velocity or temperature. It is useful to create a highly refined grid, which gives the possibility to simulate complex phenomena like high-velocity flow or flame propagation with a good accuracy, without decreasing the simulation time and with a globally finer grid. A good AMR algorithm should increase the grid resolution where the sub-grid field is the largest or in the part of the flow field in which it is most under-resolved [5].

The sub-grid field in case of a scalar can be defined in the following way

$$\phi' = \phi - \bar{\phi}. \quad (3.12)$$

Here the sub-grid scale is equal to the difference between  $\phi$ , the actual scalar field, and  $\bar{\phi}$ , the resolved scalar field. It is possible to express for any scalar the sub-grid in form of infinite series. Unfortunately, only the first term of this series can be evaluated, and it can be used to approximate the sub-grid field:

$$\phi' \cong -\alpha_{[k]} \frac{\partial^2 \bar{\phi}}{\partial x_k \partial x_k}. \quad (3.13)$$

For a rectangular cell  $\alpha_{[k]} = \frac{dx_k^2}{24}$ .

This equation can be easily generalized for a vector field (e.g. velocity, number of parcels per cell, temperature, void fraction, species, passives, or boundary (y+)). A cell is embedded if the absolute value of the sub-grid field is above a user-specified value.

Conversely the embedding is removed if the absolute value of the sub-grid is lower than 1/5 of the value specified by the user. It is possible to define different AMR sub-grid criterion and different AMR embedding scale for each condition. Moreover, it is possible to specify the time to start and stop the AMR for each field, like for boundary and fixed embedding timing control [5].

An example of AMR is presented in **Figure 3-8**.

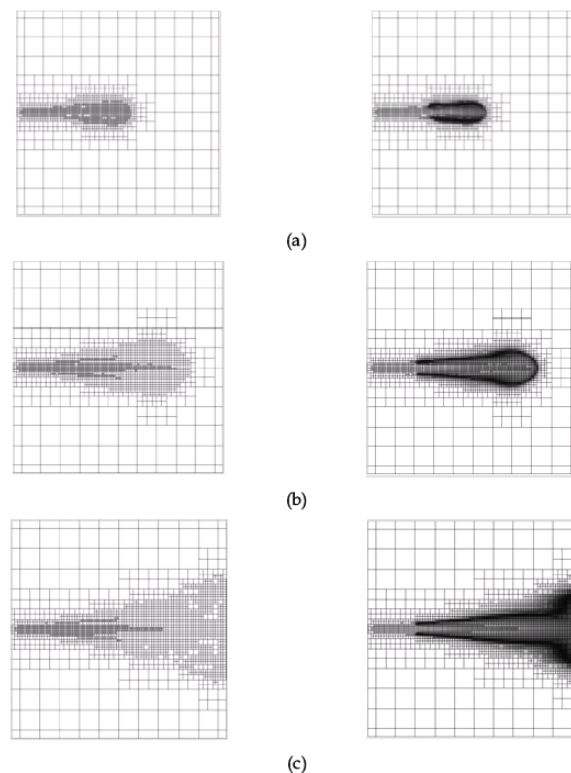


**Figure 3-8** Evolution in time of a combustive spray bomb [5]

## 3.4 COMBUSTION MODELING

In this paragraph are discussed two kind of combustion models:

- SAGE model.
- FGM (Flamelet Generated Manifold) model.

A brief overview of the two models is presented below.

### 3.4.1 SAGE model

CONVERGE models the chemical kinetics through a set of CHEMKIN inputs files. A chemical reaction is composed by a series of elementary reactions, and the complete set will describe the combustion chemical reactions. SAGE is able to calculate the reaction rate of each reaction and at the same time the CFD solver uses this information to solve the transport equations. This model is very accurate and can be used either for constant pressure or constant volume combustion.

It is possible to describe a multi-step chemical reaction through this formulation:

$$\sum_{m=1}^M v'_{m,r} \chi_m \leftrightarrow \sum_{m=1}^M v''_{m,r} \chi_m, \text{ for } r = 1, 2, \dots, R \quad (3.14)$$

Where  $R$  is the total number of reactions,  $v'_{m,r}$  and  $v''_{m,r}$  are respectively the stoichiometric coefficients for reactants and products for species  $m$  and reaction  $r$ , and  $\chi_m$  represents the chemical symbol for the species  $m$  [5].

It is possible to write also the net production rate for species  $m$ :

$$\dot{\omega}_m = \sum_{r=1}^R \nu_{m,r} q_r, \text{ for } m = 1, 2, \dots, M \quad (3.15)$$

$$\nu_{m,r} = \nu''_{m,r} - \nu'_{m,r}. \quad (3.16)$$

Here,  $M$  represents the total number of species and  $q_r$  is the rate of progress variable:

$$q_r = k_{fr} \prod_{m=1}^M [X_m]^{\nu'_{m,r}} - k_{rr} \prod_{m=1}^M [X_m]^{\nu''_{m,r}}, \quad (3.17)$$

where  $[X_m]$  represents the species  $m$  molar concentration,  $k_{fr}$  and  $k_{rr}$  are respectively forward and reverse Arrhenius rate coefficients for reaction  $r$ .

The objective is to solve the mass and energy governing equations for each computational cell. Respectively, the final results for mass and energy conservation for constant volume are:

$$\frac{d[X_m]}{dt} = \dot{\omega}_m, \quad (3.18)$$

$$\frac{dT}{dt} = \frac{V \frac{dp}{dt} - \sum_m (\bar{h}_m \dot{\omega}_m)}{\sum_m ([X_m] \bar{c}_{p,m})}. \quad (3.19)$$

Here  $\bar{h}_m$  is the molar specific enthalpy and  $\bar{c}_{p,m}$  is the molar constant-pressure specific heat.

For more information about the complete set of equations useful to reach the final formulations, check [\[5\]](#).

The **equations 3.18** and **3.19** must be solved at each computational time step. It is important to underline the difference between the temperature calculated in the equation 3.19 and the cell temperature. In fact, the first one is used only to update the rate coefficients. However, CONVERGE updates the cell temperature only after

the chemistry calculation has reached a convergence using the calculated species concentrations.

### 3.4.2 FGM model

FGM model is used in order to reduce to two scalars the reaction mechanism. In this way, the computational time, compared to SAGE model, is reduced. This model is able to capture some kinetic phenomena like flame quenching, flame extinction and ignition and to provide accurate information about emissions, fuel effects and flame dynamics. The two scalars typical of the Flamelet Generated Manifold model are:

- $Z_{FGM}$ , that represents the mixture fraction, or better the normalized ratio between oxidizer and fuel.
- $c$ , that represents the reaction progress variable.

The first one has a specific value at each cell and at each time step. It can be expressed by the following formulation:

$$Z_{FGM} = \frac{(Z - Z_{oxidizer})}{Z_{fuel}}, \quad (3.20)$$

where  $Z_{FGM}$  can oscillate between 0 and 1.

The second one also oscillates between 0 and 1 and is define as:

$$c = \frac{\sum \alpha_k \gamma_k}{\sum \alpha_k \gamma_k^{eq}}, \quad (3.21)$$

where  $\gamma_k$  is the species mass fraction and  $\alpha_k$  is a constant different for each reactants, it is set equal to zero for most of them. Only for  $CO$  and  $CO_2$  it is recommended to define it equal to one.

If the FGM model is chosen, CONVERGE starts to populate a look-up table, based on different resolution parameters. Inside the look-up table can be present the information about  $Z_{FGM, c}$ , enthalpy, pressure and  $Z_{FGM}$  variance, written in binary format. Then FGM uses the solution for the mentioned parameters to solve the needed equations.

### 3.5 EMISSION MODELING

CONVERGE contains several models to simulate soot or NOx production. Species of interest such as CO, CO2, and unburned hydrocarbons are always calculated or interpolated in CONVERGE, provided they are included in the reaction mechanism file and are a part of the combustion model used by the simulation.

#### 3.5.1 NOx modelling

In CONVERGE is possible to apply two different NOx models: thermal NOx and prompt NOx.

The first model is based on the Extended Zeldovich mechanism, used to evaluate the NO formation. This mechanism is based on the following reactions:



Thank to these reactions, it is possible to evaluate the rate of formation of NO, which can be written as:

$$\frac{d[NO]}{dt} = \frac{2R_1[1 - ([NO]/[NO]_e)^2]}{1 + ([NO]/[NO]_e)^{R'}}, \quad (3.25)$$

$$R' = \frac{R_1}{R_2 + R_3}, \quad (3.26)$$

$$R_1 = k_{R1,r}[NO]_e[N]_e, \quad (3.27)$$

$$R_2 = k_{R2,f}[N]_e[O_2]_e, \quad (3.28)$$

$$R_3 = k_{R3,f}[N]_e[OH]_e, \quad (3.29)$$

where  $[X]$  represents the molar concentration of the generic chemical compound, the subscript  $e$  refers to the equilibrium conditions,  $k$  represents the speed of reaction and finally, the two subscripts  $f$  and  $r$  denotes respectively a forward and a reverse reaction (e.g.  $k_{R1,r}$  is the speed of the reverse reaction R1).

The prompt mechanism is able to identify the formation of nitrogen monoxide in fuel-rich and low-temperature conditions. This mechanism is mostly used for gas turbine, staged combustion applications and surface combustion [5].

In order to solve the reaction rates, the De Soete global kinetic parameter is used:

$$\frac{d[NO]}{dt} = r_{NOx} - r_{N_2}, \quad (3.30)$$

where  $r_{NOx}$  and  $r_{N_2}$  represents respectively the overall prompt NOx formation rate and the overall molecular nitrogen formation rate.

During the initial stages of the flame, prompt NOx forms in a fuel-rich environment where the concentration of O is high, the N radical primarily forms NOx instead of nitrogen. Thus, the rate of prompt NOx formation is approximately equal to the rate

of overall prompt NO<sub>x</sub> formation. The phenomena described is represented in the equation 3.23:

$$\frac{d[NO]}{dt} = f k_{pr}' [O_2]^a [N_2] [fuel\ species] \exp^{-E_a'/RT}. \quad (3.31)$$

Here  $f$  is a correction factor which improves the performances of the model for fuels with higher hydrocarbon content and in fuel-rich conditions. This factor accounts for the effect of fuel type and air-to-fuel ratio. The correction factor  $f$  is used for equivalence ratio values in between 0.6 and 1.6 and it represents a curve fit to experimental data [5].  $E_a'$  is the activation energy of the reaction, directly connected to the temperature. In general, higher  $E_a'$  means higher temperature to start the reaction.

For a more detailed scenario about NO<sub>x</sub> formation, is recommended to read [5].

There is also the possibility to calculate NO<sub>x</sub> using the SAGE detailed chemistry solver, by specifying the reactions in the mechanism data file (e.g., mech.dat) and the thermodynamic data file (e.g., therm.dat) to model NO or both NO and NO<sub>2</sub>. The results given by the two methods are slightly different, because of the simplification applied in the model.



## 4 COMBUSTION AND FLAME STABILITY

Different requirements must be satisfied by a generic combustor [7]:

- High-combustion efficiency.
- Reliable and smooth ignition.
- Low pressure loss.
- Wide stability limits.
- Outlet temperature distribution able to maximize the lives of the nozzle guide vanes and turbine blades.
- Size and shape consistent with engine envelope.
- Freedom from manifestations of combustion instability like pressure pulsations.
- Low pollutant emissions.
- Design for minimum cost and manufacturing simplicity.
- Durability.
- Maintainability.
- Petroleum, biomass-based and synthetic multifuel capability.

For industrial engines, multifuel capability and long operating life, together with low pollutant emissions and low fuel consumption, are the most important requirements.

## 4.1 COMBUSTOR DESIGN

It is necessary to have a wide range of combustor layouts. This task is important in order to face two different aspects:

- There is a wide range of engines design.
- The space available inside the engine must be used as effectively as possible.

A generic geometry for the combustion chamber is presented in **Figure 4-1**.

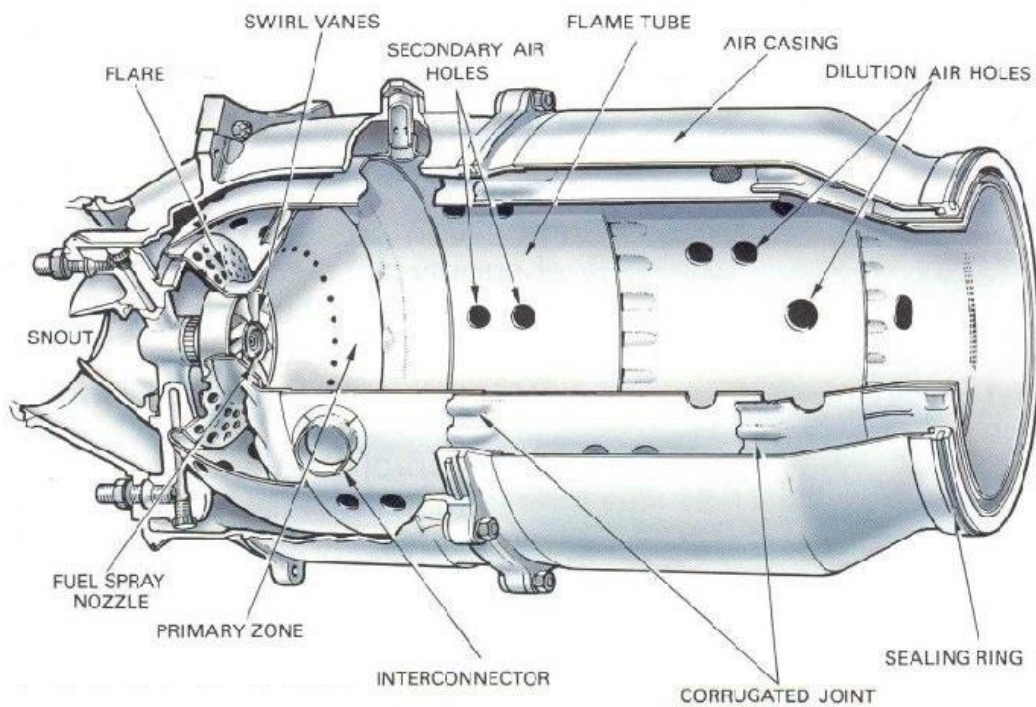


*Figure 4-1 Example of gas turbine combustor, by Rolls Royce [8].*

### 4.1.1 Combustor types

Typically, the combustor can be (**Figure 4-2**):

- Tubular (or can).
- Annular.
- Turboannular or can-annular.

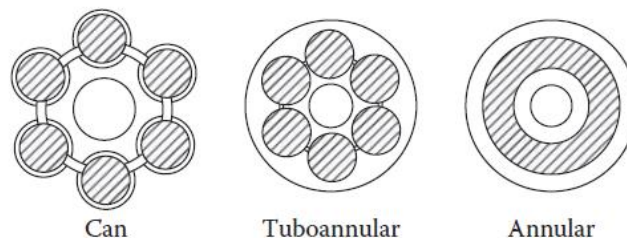


*Figure 4-2 Section of the three main combustor types [7].*

The first type of combustor is composed by a cylindrical liner inside a cylindrical casing. The two elements are mounted concentrically, in order to have a homogeneous effect of creep and fatigue phenomena on the combustor surface.

The main advantage of these systems is that they require relatively a limited amount of time and money for their development. However, the excessive weight and length of these combustors make impossible their use in aircraft engines. In fact, they are mainly used in industrial units where it is necessary to guarantee accessibility and simplicity in maintenance [7].

In the second type of combustors is present an annular liner, which is located inside an annular casing. The two elements are also concentric. Thanks to its clean design, this kind of combustor is characterized by a compact structure and lower pressure

losses. The heavy buckling load, which affects the outer liner, is the main drawback. Moreover, for large annular combustors, the cost of supplying air for the required testing temperature, pressure and flow rate, is generally high.

Finally, the tuboannular combustor, presented in **Figure 4-3**, is composed by a series of tubular liners, generally from 6 to 10, which are all located inside an annular casing.

If compared with the annular, the tuboannular design has a fundamental advantage. In fact, chamber development can be obtained with a limited air supplies, using just a small part of the total structure containing one or more liners. The main drawbacks come out when trying to reach a consistent airflow pattern [7].

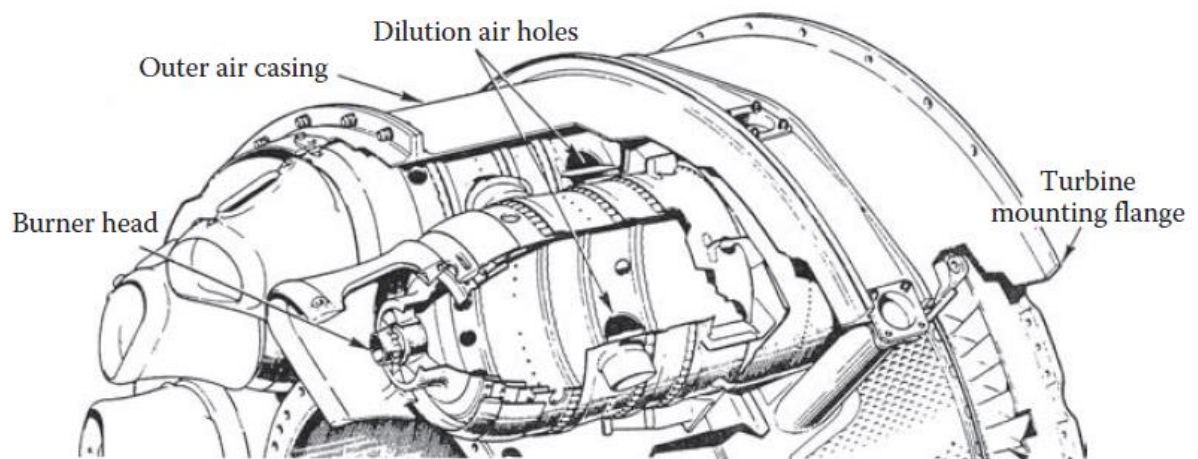


**Figure 4-3** *Tuboannular combustor arrangement* [7].

### 4.1.2 Diffuser

The diffuser is fundamental in order to decrease the combustor inlet velocity value and consequently the pressure losses. Moreover, it is important to guarantee a smooth and stable flow inside the liner and to recover a part of the dynamic pressure.

Typically, the diffusers can follow two different philosophies:

- “Aerodynamic” diffuser.
- “Bump” or “step” diffuser.

The first one is used to achieve maximum recovery of the dynamic pressure. The first section of the aerodynamic diffuser is positioned at or near the compressor outlet. The objective is to achieve a velocity reduction, typically about 35%, before the air divides into three different passages.

The second one is characterized by a short conventional diffuser, which is able to decrease the inlet air velocity of the 50%. A representation of the two kind of diffusers is shown in **Figure 4-4**

In the case studied, the air is not flowing into different passages, thanks to the reverse flow of the compressor air, which allows the initial division of the air into the different holes.

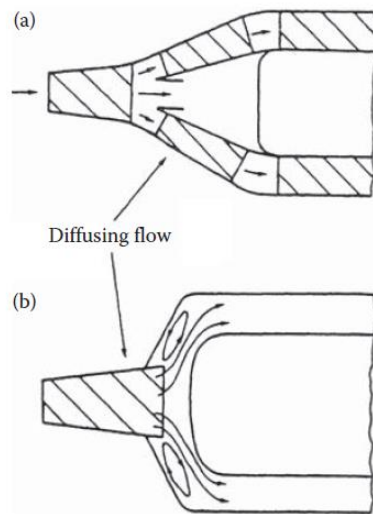


**Figure 4-4** Two basic examples of (a) aerodynamic and (b) bump diffusers [7].

Both types of diffusers are used. Dump diffusers are actually preferred because of the higher possibility hardware dimensions and inlet velocity profile variations [7].

## 4.2 COMBUSTION ZONES

Every combustion process is composed by three phases, which can be identified by three different zones:

- Primary zone.
- Intermediate zone.
- Dilution zone.

These three phases are connected to these zones, because they can be physically identified in a certain position of the combustor, moving respectively from the diffuser (where the combustion starts) to the outlet. At the outlet the reactions are frozen, and the pollutant will move to the turbine, through the transition piece.

It is crucial to identify these three phases along the liner, to state that the combustion process is evolving in the right way. An overview of the combustor zones is in **Figure 4-5**

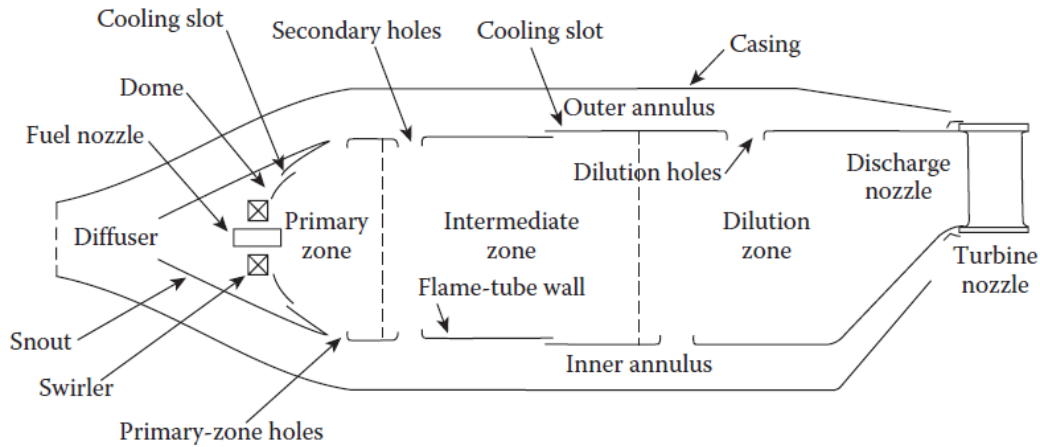


*Figure 4-5 Main components of a conventional combustor [7].*

#### 4.2.1 Primary zone

The primary zone is fundamental in order to fix the flame and provide sufficient temperature, time, and turbulence, useful to reach the complete incoming fuel–air mixture combustion [7].

In this zone, can be identified different flow patterns, but they are all characterized by the presence of a toroidal reversal vortex, which recirculates a part of the hot combustion gasses or of the mixing air. This vortex is important in order to help the swirler to promote the mixing and so to provide a continuous ignition.

Here the temperature can reach locally more than 2000 K. This will result in dissociation reactions, which will create a huge concentration of hydrogen and carbon monoxide in the exhaust gases.

### 4.2.2 Intermediate zone

The intermediate zone is fundamental in order to gradually decrease the temperature of the gases, instead of decreasing it brutally because of the massive addition of air typical of the dilution zone. Here the average temperature remains around 1800 K.

In this zone the temperature is decrease to an intermediate level, thanks to the continuous addition of small quantities of air. This process helps the burnout of soot and gives the possibility to some pollutants, like CO and UHC (unburned hydrocarbons), to proceed to completion of the combustion [7].

Is fundamental to manage the CO and unburned hydrocarbons emissions, because they are a source of combustion inefficiency.

### 4.2.3 Dilution zone

It is useful in order to admit the air from the dilution and cooling channels. Here the temperature will decrease to a value lower than 1500 K, in order to be sent to the turbine inlet. This phase is important in order to avoid the damage of the turbine.

Generally, from 20% to 40% of the total air entering in the combustor is available for dilution. This percentage of air is introduced in the liner through one or more holes, generally disposed in rows. The shape and the size of these holes are studied to optimize the air penetration and so the mixing with the hot gasses stream [7].

The flow pattern for a generic combustor chamber is shown in **Figure 4-6**.

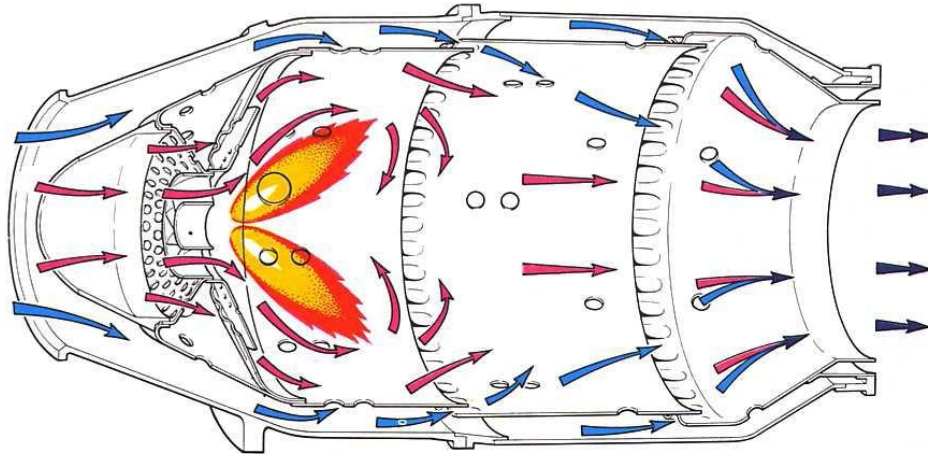


*Figure 4-6 Example of flow pattern for a generic combustion chamber [9].*

### 4.3 FUEL INJECTION

The gas injection is based on the usage of an injector. The injector is characterized by some features, which are fundamental to be studied in order to obtain a good mixing and flame stability:

- Diameter of the injector holes;
- Spray angle;
- Distance between swirler and injector holes.

The diameter is influencing the speed and the pressure of the gas, while the other two parameters are important in order to guarantee a good volumetric distribution, which will influence the mixing and so will promote the start of the combustion. The injector-swirler used for this project is presented in **Figure 4-7**.

### 4.3.1 Gas injection

Gas injection is generally based on plain orifices and slots plus a swirler. In particular for low heat content gases, there are some problems connected to the combustion process. A problem can be the fuel mass flow, generically around one fifth of the total one. This can create a mismatch between turbine and compressor.

Another problem is their low burning rate, which may need a larger volume for combustion, over the extra volume useful to accommodate the fuel flow. It can also be difficult to achieve the needed mixing rate in the zone in which the combustion starts. If the mixing rate is too high, there are poor lean-blowout characteristics. If the mixing rate is too low it is possible to have a rough combustion [7].

Anyways, for high calorific value gas fuel, like natural gas, the combustion process is less sensitive to these aspects.

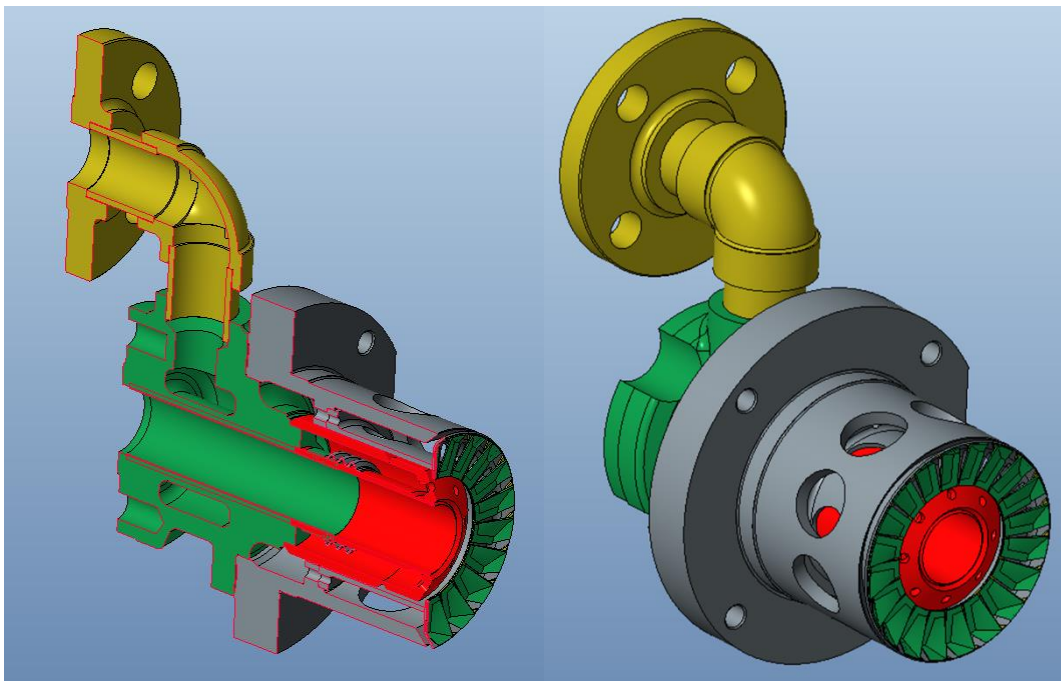


*Figure 4-7 Complete view and section view of the injector-swirler, courtesy of EthosEnergy.*

## 4.4 WALL COOLING

The principal role of the liner is to contain the combustion process in the prescribed area and to guarantee a good distribution of air to all the combustor zones. To accomplish these tasks, the liner must be sufficiently strong to withstand the variation of pressure due to the ignition. It must have also a good resistance to the temperature variation, in order to avoid creep rupture.

The last problem is important, because of the continuous contact with high temperatures which are evolving in time during the combustion process. For this reason, the combination of an oxidant-resistant material, characterized by a good resistance to the high temperatures, and the cooling air effect, plus some surface treatment useful to increase the high temperature resistance, are used.

Generally, more than the 20% of the entire air coming from the compressor, is used for cooling. It is possible to evaluate the liner wall temperature, thanks to a balance between the heat that the liner transfers to the casing by radiation and to the annulus air by convection, and the heat that it receives by convection and radiation from the hot gasses.

An increase in pressure ratio can create some problems in cooling effect. In fact, it is actually beneficial in reducing the specific surface area to be cooled, but it will create an increase in inlet air temperature, which will oppose to the cooling effect [7].

## 4.5 COMBUSTION FUNDAMENTALS

Combustion process is described as an exothermic reaction between fuel and an oxidant. In gas turbines, the fuel can be either liquid or gaseous, the oxidant is always air.

The combustion process may occur in different forms, and it is not always characterized by the presence of flame or luminescence. The release of energy, due

to the chemical reactions, is a crucial step in the combustion process. However, in high temperature flames the energy release is very quick and can be disregarded.

#### **4.5.1 Deflagration**

Deflagration is the typical energy release process in gas turbines. This process is really fast, in fact it requires only 1 ms to reach the 80% of completion, and it is based on the propagation of the flame through the unburned mixture of air and fuel. From the chemical point of view, a flame can be defined as a fast chemical change which happens in a thin layer of fluid, characterized by temperature, species concentration gradient and also luminescence. It is also possible to define the flame front as the interface between burned and unburned gasses, which gives the possibility to define the deflagration waves propagation.

Deflagration burns outward radially and requires fuel to spread. The speed at which deflagration moves depends on the quality of the available fuel, but as definition, it is always lower than the speed of sound.

### **4.6 FLAME CLASSIFICATION**

Flames are divided in two main classes:

- Premixed flames.
- Diffusion flames.

This distinction is connected to the way in which air and fuel are mixed. In premixed flame, as suggested by the name, air and fuel are homogeneously mixed before the combustion process. In diffusion flame the mixing occurs by diffusion in the flame zone. Depending on the flame velocity, both can be turbulent or laminar.

In premixed flames, after the flame ignition, flame will move throughout the entire combustible mixture volume. The factors which affects the rate of propagation of the flame (e.g. turbulence) are important in order to define the design parameters of a combustion system.

To describe the diffusion flame can be used the example of a candle. Fuel vapor moves from the wick, but it starts to burn only if it can mix with the oxygen which is present in the air. Generally, for this kind of flame, the fuel/air mixing limits the overall combustion rate [7].

## 4.7 FLAMMABILITY LIMITS

The success of the burning process is always connected to the composition of the mixture. To encourage the combustion process, the air-fuel must be in a certain range, between the lean limit and the rich limit. If the air-fuel ratio is out from this range, the mixture will not burn. This range can be influenced by an increase in pressure above the atmospheric one, which will increase the rich limit and let easier the start of combustion. The lower limit is less influenced for a pressure increase lower than 5 Mpa. Also, an increase in pressure can enlarge this range, but the effect of temperature is lower than the pressure one. The flammability limits for gas methane are in **Figure 4-8**.

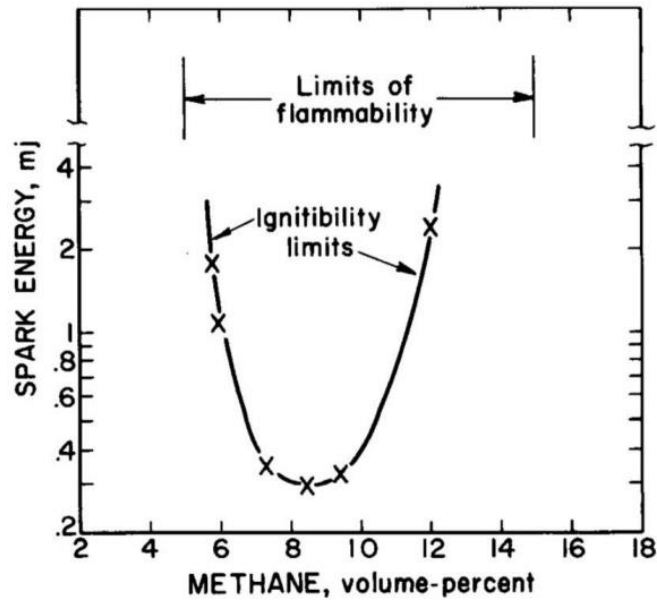


Figure 4-8 Flammability limits of methane [10].

## 4.8 FLAME STABILIZATION

The stability of a flame can be associated to two different aspects:

- The description of the fuel/air ratios useful to reach a stable combustion.
- The measure of maximum air velocity that can be tolerated by the system before flame extinction.

Both these properties have an important influence on the final flame stability. So, it is fundamental to try to work in a stability range of combustion that must be as large as possible, and also the blowout velocity should be high. In gas turbine chambers in general the first aspect is the most important one

### 4.8.1 Measurement of stability performance

In order to study a combustion chamber or to develop a new one, it is crucial to perform a series of extinction tests, with a constant value of inlet temperature and pressure of air. The final purpose of these tests is to define the stability loop of the system, and so to validate it. An example of stability loop is presented in **Figure 4-9**.

It is described the procedure used in the mentioned tests:

1. Fuel is injected and the mixture is ignited.
2. Fuel flow is slowly reduced and flame extinction occurs (lean extinction).
3. Combustion is re-established and fuel flow is gradually increase until extinction occurs (rich extinction).
4. The process is repeated for higher air mass flow values, until the stability loop can be drawn.

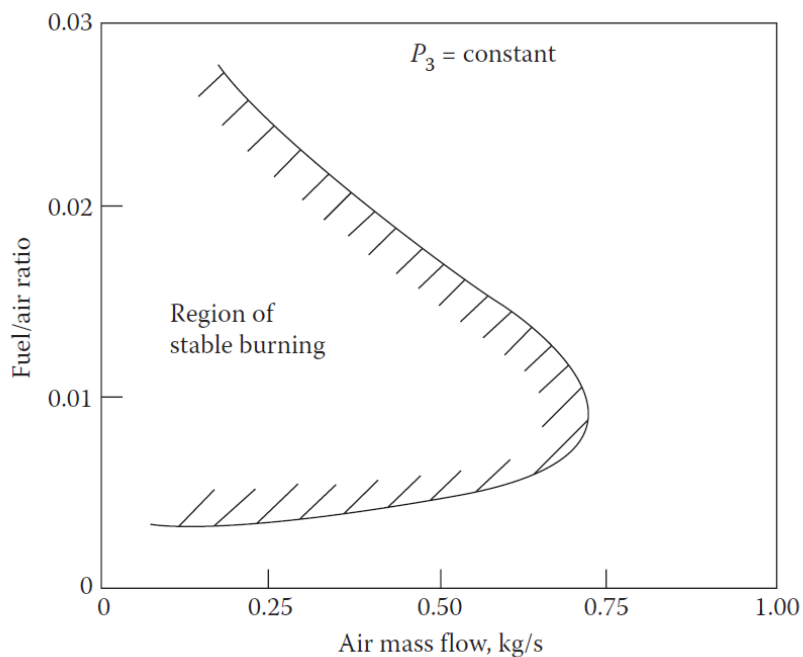


**Figure 4-9** Example of combustion chamber stability loop [7].

Then, these tests are also performed varying pressure, in order to evaluate the stability performances for each working condition. As said in the paragraph 4.7, an increase of pressure will extend the fuel/air ratio, particularly on the rich side, and this effect will give a bigger stability range, as showed in **Figure 4-10**.

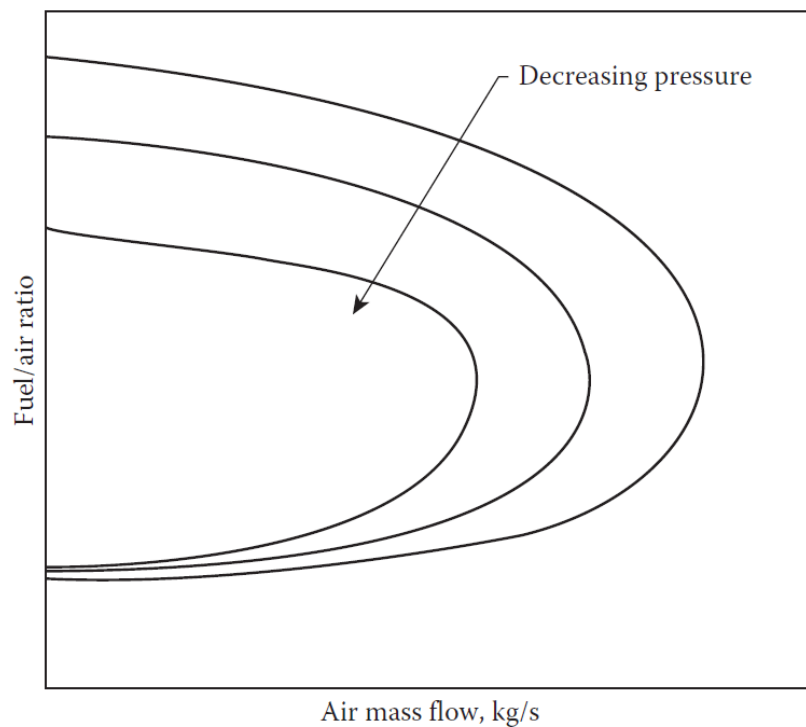


**Figure 4-10** Influence of pressure in the stability loop [7].

Another method used to determine the flame stability is the Water Injection Technique, generally cheaper than the first one. In the figure below is presented the workbench used to perform the stability loop test.

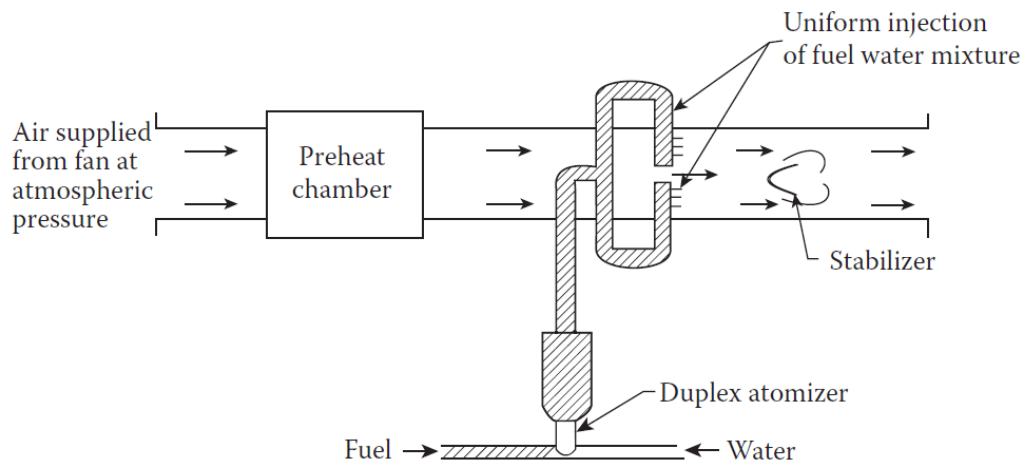


**Figure 4-11** Water injection rigs for stability tests [7].

The procedure is:

1. Is supplied air at atmospheric pressure using a fan. The introduction of water will simulate low pressure.
2. Temperature and velocity of the gas are continuously adjusted in order to respect the desired values.
3. Fuel is injected and flame is established downstream the stabilizer, in the recirculating zone.
4. Water is gradually injected until the flame extinction.
5. The process must be repeated for different fuel flows until a complete stability loop can be drawn.

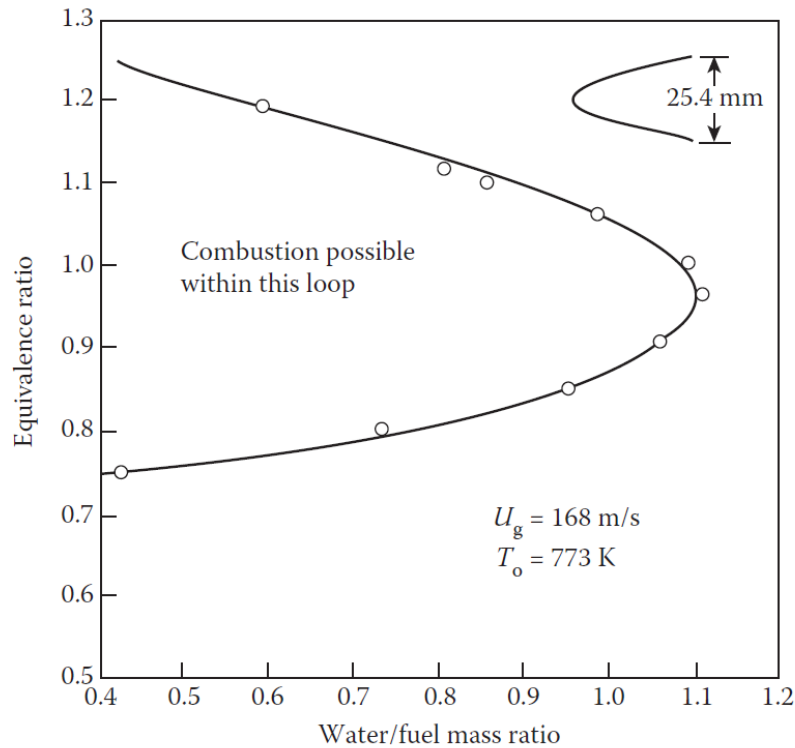


Figure 4-12 Typical water injection stability loop [7].

#### 4.8.2 Bluff-Body Flameholders

The Bluff-Body Flameholders are typically used to stabilize the flame in flowing combustible mixtures, in particular in turbojet afterburner systems. Its use is fundamental in order to define the parameters to obtain a good stability of the flame, so theoretical and experimental methods have been developed. Actually, are used some equations in order to predict the limits of stability in terms of temperature, pressure, velocity, bluff-body dimensions, turbulence, blockage ratio and equivalence ratio. The large number of variables which are influencing the stability of the flame underlines the importance and difficulties related to this problem.

For more information about the different methods and the experimental analysis, it is suggested to consult [7].

### 4.8.3 Stability limits

The stability properties of the bluff-body stabilizer have been studied in terms of homogeneous or heterogeneous air-fuel mixtures. The experimental results of these studies have given some important conclusions about the factors that can extend the stability limits. They are [7]:

- Increase the approach steam velocity.
- Reduce the approach steam temperature.
- Increase gas pressure.
- Reduce turbulence intensity.
- Approach unity in equivalence ratio.
- Increase flame holder size and base-drag coefficient.
- Reduce flame holder blockage (for defined size).

### 4.8.4 Combustion chamber flame stabilization

Flame stabilization for combustion chamber has not been studied in the same way of bluff-body Flameholders, but there are some rules which remains fundamental in order to guarantee a good flame stability.

The first rule is to inject air form a small number of large holes. This is important because large holes will produce a large jet with a large recirculation flow. Thanks to this second effect, ample time for combustion is provided. Naturally, in order to increase the hole size, the number of holes must decrease. So, it is important to calibrate these values.

The second element which can influence the flame stability is the amount of air that enters in the recirculating zone through the apertures in the liner wall. The design of these apertures can control the amount of air that participate to the primary combustion.

Another essential feature to guarantee a stable flame is the toroidal reversal flow, located near the swirler, primary zone, shown in **Figure 4-13**, and alimented by the air passing through it. This zone is fundamental for two main reasons:

- Here is the main heat release to start the combustion.
- Here is a recirculation of burned and burning gasses, that mix with the incoming air. In this way the combustion is continuously alimented.

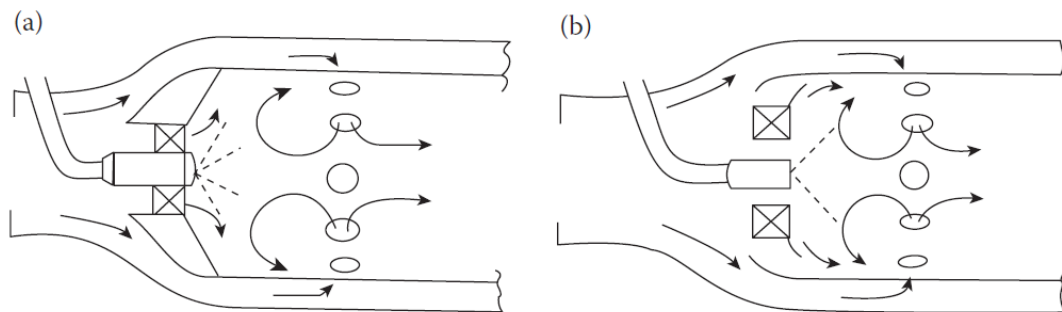


**Figure 4-13** Example of primary zone for tubular (a) and annular (b) combustors [7].

Another important factor in flame stabilization is the mode of fuel injection, in particular to manage the lean blowout limit. The poor fuel distribution typical of pressure-swirl atomizers ensures the start of combustion also for mixtures that are richer than the average value. So, also if the average fuel-air composition is under the lean blowout limit, the combustion will not stop thanks to the presence of richer, in this case near-stoichiometric, mixtures.

In opposition air blast atomizers, will provide a better fuel-air mixing but the burning limits are unfavorable.



# 5 MODEL CREATION AND CALIBRATION

As said in the chapter one, the objective of this project is to develop and calibrate a model able to simulate the behavior of an existing industrial gas turbine burner, in order to obtain precise pollutant predictions.

In order to reach this objective, the following workflow has been developed:

- 1) Creation of the 3D model, with appropriate modifications due to the implementation in CONVERGE;
- 2) Fixing of geometry errors;
- 3) Definition of the boundaries on the final geometry;
- 4) Implementation of the case setup;
- 5) Simulations and analysis of the 2D and 3D results.

Below is described in detail the entire procedure.

## 5.1 3D MODEL

The 3D model of the FIAT TG20 B-7/8 has been developed using Pro/ENGINEER, a 3D CAD modelling software created by PTC (Parametric Technology Corporation) [11]. The first release of this model has been produced by the designers of the company EthosEnergy Spa. This first release was characterized by the following problems:

- The 3D model had been produced following the real production workflow. For this reason, it was composed by a series of laminar sheets welded one to

each other. This kind of geometry will create diagnostic problems on converge which will naturally prevent the simulation to start.

- The model was characterized by a high complexity and by the presence of a high amount of elements which had been considered useless for the CFD analysis (e.g. disks, bolts and relative holes useful to connect the burner and the compressor).
- The CAD file had to be transformed in a high quality STL file, in order to be correctly imported in CONVERGE.

For all these reasons, it was necessary to develop a new CAD file. The final release has been produced using the same software and is characterized by the below features:

- The entire surface of the final model comes from a continuous and unique element.
- All the bodies that are not influencing the fluid flow have been eliminated
- The final geometry has been simplified in order to manage it easily in CONVERGE.

In the **Figure 5-1** and **Figure 5-2** are reported the first and the last release, to better understand the modifications mentioned.

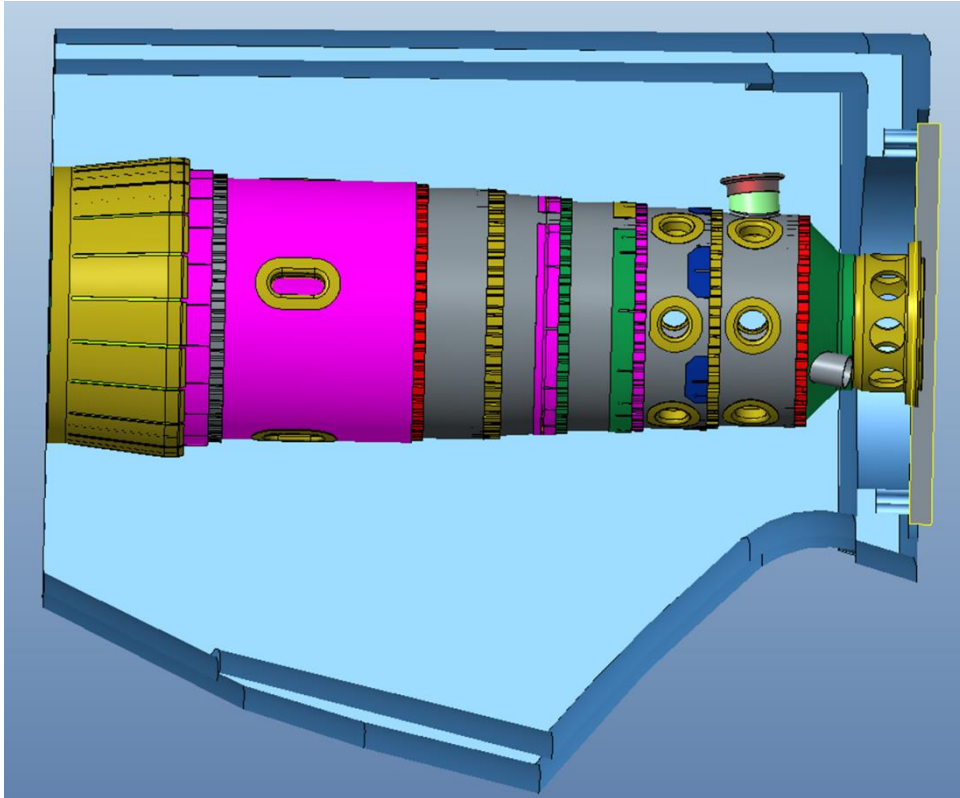


*Figure 5-1 Initial geometry, courtesy of EthosEnergy*

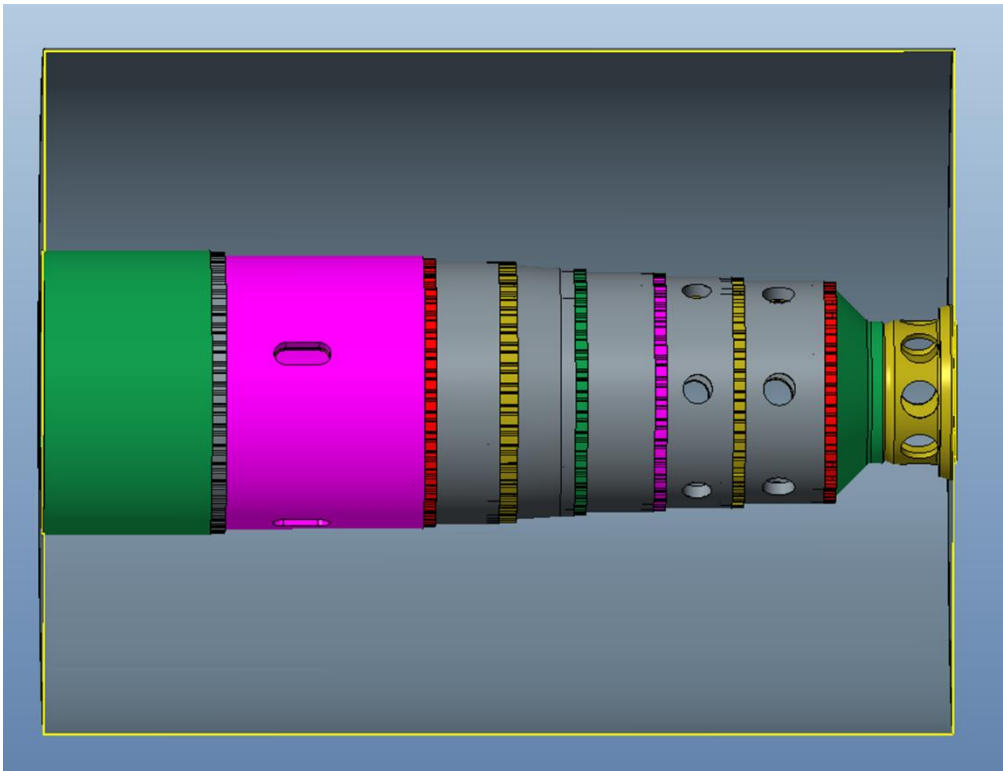


*Figure 5-2 Simplified geometry*

The geometry is characterized by three macro bodies:

- The external body is the casing. It is able to take the air coming from the compressor and let it recirculate inside the burner, thanks to a backflow recirculation. The temperature and the pressure inside the casing can be considered as equal to the ones at the outlet of the compressor.
- Along the entire length there is the burner. The burner length is 99.2 cm and the maximum diameter is 33 cm. It is characterized by 7 rings of cooling channel, with a trapezoidal section, a series of 8 mixing holes and 3 series of dilution holes, the first and the second series are composed by 6 holes, the last one by 4 holes (following the positive z direction). The air that is entering in the casing will automatically distribute inside the holes, thanks to the differences in diameter and internal pressure. The fluid which enters in the mixing holes, is the one that will mix with the gas methane. The air entering from the dilution holes has two different tasks. First of all, it is fundamental in order to decrease the peak of temperature along the burner, in order to avoid a dangerous temperature at the inlet of the turbine. Then, it also increases the air-fuel ratio that initially is too low to permit the start and consequently the alimentation of the flame. Finally, the air moving inside the cooling channels is important, in order to avoid an excessive increase of temperature on the burner surface, which can cause the creations of cracks due to creep phenomena and consequently, the destruction of the burner.
- Finally, the last element is the injector. The methane is injected inside and goes out through 8 holes. The spray angle of the injector is 30°.

It is important to highlight that the entire combustor is characterized by 8 burners, so the geometry described is a simplification of a clove of the real complete geometry. This operation has been necessary in order to decrease the simulation time.

It is also important to describe the swirler. Its role is critical in order to impose a certain turbulence to the fluid, and to encourage a good mixing and a more complete combustion evolution. It is characterized by 26 inclined blades, in order to guarantee a correct turbulence of the air that is entering in the mixing holes. It is important to highlight that a small part of this air is passing in a lateral space between the swirler and the burner. This air is useful in order to cool the “swirler area”, which can be easily damaged by an incorrect combustion.

In the figures below are presented the characteristics described.

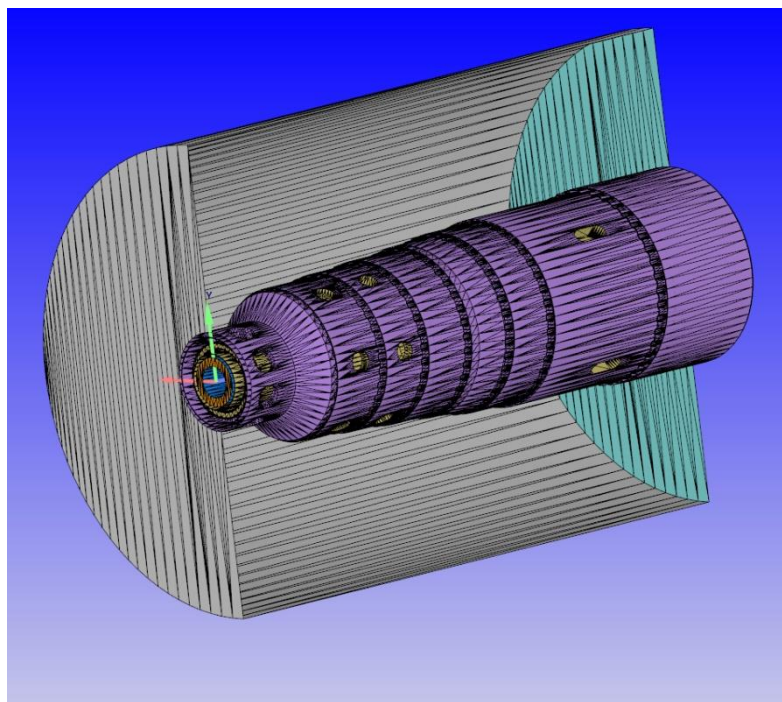


*Figure 5-3 STL file of the final geometry. The section has been performed only on the casing.*

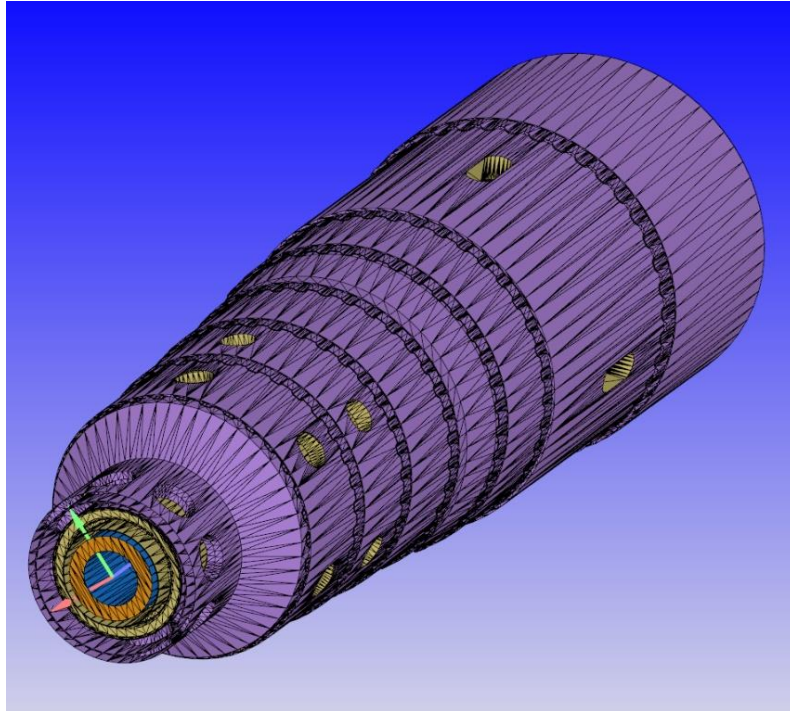


*Figure 5-4 Complete view of the dilution, mixing and cooling holes on the liner.*

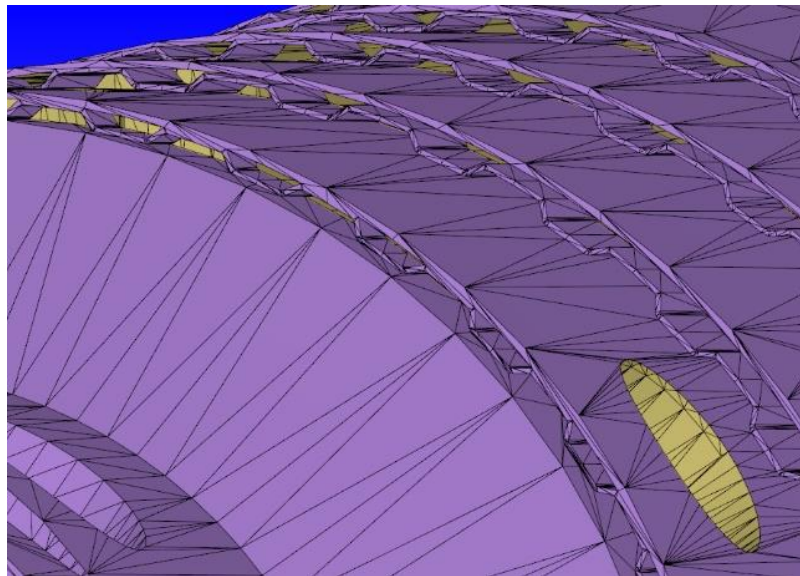


*Figure 5-5 Detail of the cooling channels.*

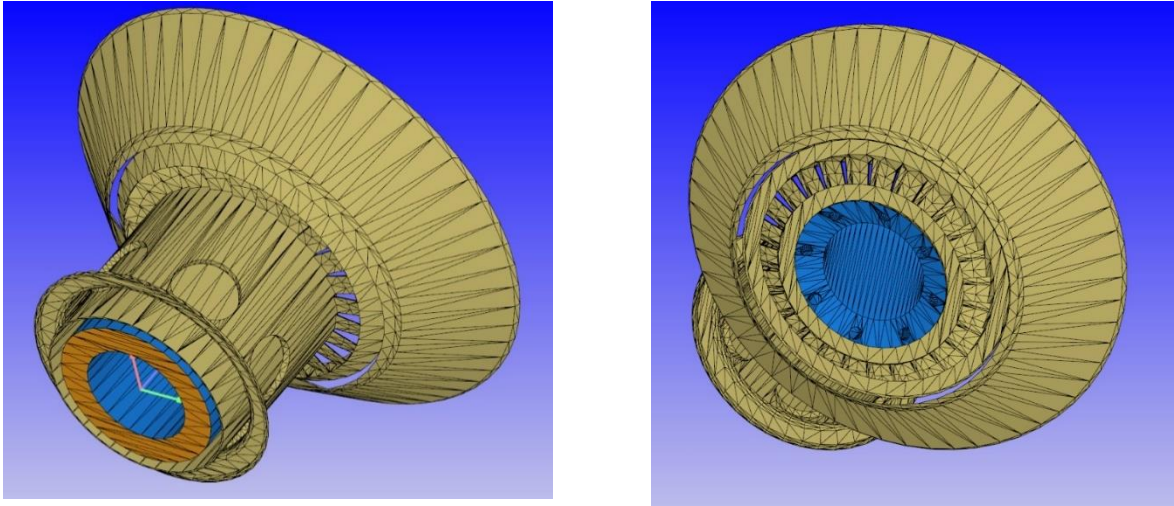


*Figure 5-6 Back and front view of injector-swirler.*

## 5.2 CONVERGE DIAGNOSIS

In order to upload the geometry in CONVERGE, is necessary to convert the file in STL. STL (an abbreviation of "stereolithography") is a file format native to the stereolithography CAD software. An STL file describes a raw, unstructured triangulated surface by the unit normal and vertices (ordered by the right-hand rule) of the triangles using a three-dimensional Cartesian coordinate system.

Unfortunately, the transformation in STL causes the following problems on the triangulated geometry:

- Triangle intersections. Here the plane of one triangle passes intersects the plane of another triangle
- Nonmanifold edges. Here an edge is shared by more than two triangles.
- Nonmanifold vertices. Here there is a vertex that connects two otherwise disconnected pieces of geometry.
- Normal orientation. Here are present some triangles whose normal vectors are inconsistent respect on the normal vectors of the adjacent triangles.

- Isolated triangles. Here there are some triangles surrounded by neighboring triangles that are all on a different Boundary ID number.
- Open edges. Here are some triangles with at least one edge that is not shared by another triangle.
- Overlapping triangles. Here there are some triangles that meet other triangles at an angle, less than the specified value, in degrees.

These errors can cause wrong results and incontinency in simulation. In particular, in CONVERGE, triangle intersections, nonmanifold problems, isolated triangles and inverse normal orientation will prevent the simulation to start.

For these reasons, CONVERGE provides a diagnosis tool, in order to fix manually these geometry problems.

The tool has been successfully used in order to eliminate intersection, nonmanifold problems and inverse normal orientation and overlapped triangles.

In the following figures are presented some examples of geometrical problems identified by CONVERGE.

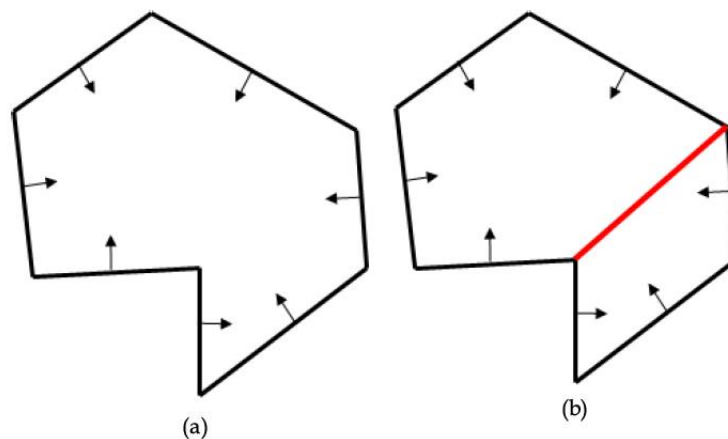


**Figure 5-7** Example of Nonmanifold edge (red line) and problem resolution (a) [5].

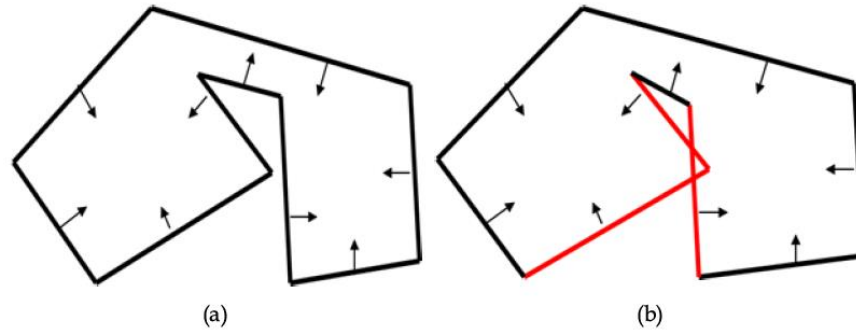


*Figure 5-8 Example of Intersecting triangles (red lines) and problem resolution (a) [5].*

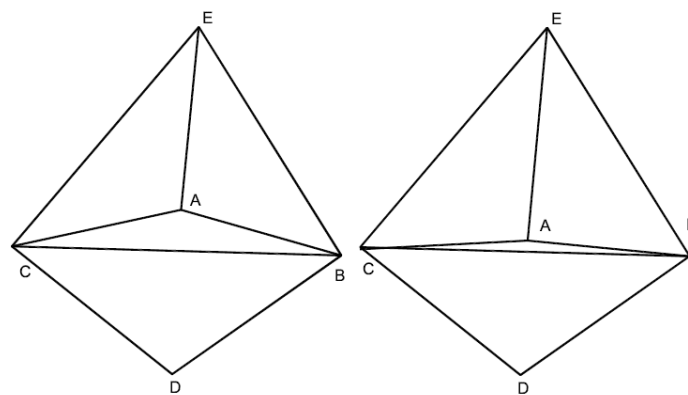


*Figure 5-9 Example of Overlapping triangles [5].*

### 5.3 BOUNDARIES DEFINITION AND CASE SETUP

After the geometry fixing, it becomes necessary to define the boundaries, in order to apply the different boundary conditions on the surface.

The different types of boundaries have been previously described in the **paragraph 3.2.**

The boundaries defined for this geometry are:

- Casing\_wall: it is characterized by the entire casing surface, except for the air inflow surface. It is a wall boundary, in which has been imposed the compressor air temperature.
- Casing\_air: it is an inflow boundary. The air is entering from this surface, moving in the opposite direction respect on the z axis. Air mass flow rate and temperature are imposed here.
- Liner\_hot and liner\_cold: are two parallel surfaces which represent the effective burner area. The external one is the liner cold, in contact with the air inside the casing. The internal one is the liner\_hot, which represent the surface directly in contact with the combustion phenomenon. For this reason, these two areas have been managed in a different way, considered as part of two different regions.
- Exit: it represents the outflow of the combustor. So, it has been identified as outflow boundary. The products of combustion are sent to the turbine through the transition piece, an “s shape” element which connects the burner exit to the turbine. Here is important to evaluate the backflow phenomenon, because of the toroidal turbulences that can be crated at the outlet.
- Injector: it is a wall boundary. This boundary includes the entire injector geometry. Here the temperature is set as equal to the one of the inflow fuel.
- Fuel\_injector: it represents the fuel inflow boundary. The methane is injected inside the injector with a pressure that must be higher than the one inside the burner. This expedient is necessary in order to guarantee the correct fluid motion.

Each boundary must be associated to a Region. A Region is a collection of one or more boundaries. CONVERGE uses regions to initialize variables (temperature, pressure, turbulent kinetic energy, turbulent dissipation, species, and passives), control the flow between portions of the geometry, and report simulation results [5].

Three regions have been identified in this project:

- Combustor region, which is composed by two different boundaries, liner\_hot and exit. It is called Region 0.

- Casing region, which is composed by casing\_wall, casing\_air and liner\_cold. This is the Region 1.
- Injection region, or Region 2, which includes the injector and fuel\_injector boundaries.

As said before, in each region are set the starting variables of the simulation, different from the BCs.

In order to create a connection between the regions, it has been imposed an open event. CONVERGE uses events to active or deactivate the disconnect triangles, which are automatically created by CONVERGE to close the gaps between two connected regions and control when and where flow between regions is allowed. An open event deactivates the disconnect triangles and thus allow flow between the specified regions [5].

After the boundary definition, the case setup can be draw up.

It is composed by different sections, which must be all set carefully, in order to obtain a more realistic result. The sections are:

- Materials.
- Simulation parameters.
- Boundary conditions.
- Initial conditions and Events.
- Physical models.
- Grid control.
- Output/Post-Processing.
- Advanced parameters.

In the next paragraphs the characteristics of these sections are explained. The Boundary conditions, initial conditions and events sections have been just discussed in this paragraph.

### **5.3.1 Materials**

In this first section, the species that are involved in the combustion are defined, together with the reaction mechanism and thermochemical data. The mechanism used to model the combustion process of methane is the GRI-mech 3.0 [12]. It is characterized by 325 reactions and 53 different species, and each specie is connected to a certain variation in thermochemical parameters for a temperature variation. In this way, the fluid characteristics are always known. GRI-mech is not the only reaction mechanism that can be used. It has been chosen for this analysis considering that it is the faster one, because of the limited number of reactions and species, but also because it is able to guarantee a good approximation in final results.

### **5.3.2 Simulation parameters**

Here all the simulation parameters, like time parameter or CFL numbers, are defined.

It is important to set the CFL numbers in the right range, otherwise the risk is to extinguish the flame immediately. Here are also defined the start and end times of simulation, and the computational time for each time step. CONVERGE uses a variable time step algorithm, which is able to oscillate between a minimum and a maximum time step. This method will provide better results [5].

### **5.3.3 Physical Models**

In this section is possible to model the combustion, the turbulence and the emissions. Referring on the combustion model, it has been created two different case setups, using SAGE or FGM model, in order to compare them and understand which model is the best one for this kind on analysis. As turbulence model, the RANS RNG  $k-\varepsilon$  has been chosen, in order to decrease the computational time without decreasing the accuracy of the results.

Finally, the NO<sub>x</sub> emissions have been modeled using the Extended-Zeldhovic and the prompt mechanism, in order to have a complete evaluation during all the combustion phases, from rich to lean mixtures. The soot has not been modeled in this project, because the amount of soot produced by this kind of engines is really limited.

### **5.3.4 Grid control**

The fluid mesh base size is defined in this section, together with AMR and fixed embedding parameters. This section is fundamental in order to obtain a good mesh and mesh refinement in the combustion area, which will provide an increased results accuracy. The mesh size will change from 40 mm in the casing region to 5 mm in the combustor region.

Thanks to the localized and sequential mesh variation given by AMR and fixed embedding, it is possible to reach an acceptable mesh size.

### **5.3.5 Output/Post-processing**

The principal role of this section is to define the parameter values which have to be calculated by CONVERGE at each time step. So, it is fundamental to choose the parameters in the right way, in order to make a complete results analysis.

CONVERGE will produce a series of 2D plots in which each parameter is in y axis, and the time variable is on x axis. It is also able to create 3D results, analyzed using Tecplot 360 [13].

## 5.4 EXPERIMENTAL DATA

In order to validate the simulation results, some experimental data has been provided by EthosEnergy Spa. In order to make these data comparable with the ones obtained in CONVERGE, they must be slightly manipulated.

The first problem is connected to the units of measurement. CONVERGE is giving the pollutant emissions in kg/s, but the experimental results are in ppm. In order to transform the unit of measurements, it has been used the following equation [14]:

$$G_{NOx} = \frac{[NOx]_{ppm} * G_{exh} * MW_{NOx}}{1000000 * MW_{exh}}, \quad (5.1)$$

Where  $MW_{NOx}$  is the molecular weight of NOx,  $MW_{exh}$  represents the molecular weight of the exhaust gasses,  $G_{NOx}$  and  $G_{exh}$  are the mass flow rates in kg/s of NOx and exhaust gasses, respectively.  $MW_{exh}$  is considered equal to 29 kg/kMol, which corresponds to the molecular weight of air. This value is used because in general more than 90% of exhaust gasses is air, so it can be approximately considered as air.

Another correction is connected to measuring instrument. In fact, the standard imposes to set the zero of the analyzer to 3% of oxygen for gaseous fuels [15]. The formulation proposed is the following [16]:

$$[c]_n = \frac{(21 - O_{2,n})}{(21 - O_{2,m})} * [c]. \quad (5.2)$$

Here  $[c]_n$  is the normalized NOx concentration,  $[c]$  is the effective concentration, 21 represents the % of air in atmospheric area,  $O_{2,n}$  is the standard %, 15% for the standard, and finally  $O_{2,m}$  is the effective one [17]. The value normalized is equal to the effective value times 2.

$$[c]_n = 2 * [c]. \quad (5.3)$$

Now is possible to convert the experimental data. Below are presented the experimental results, provided by EthosEnergy [18]:

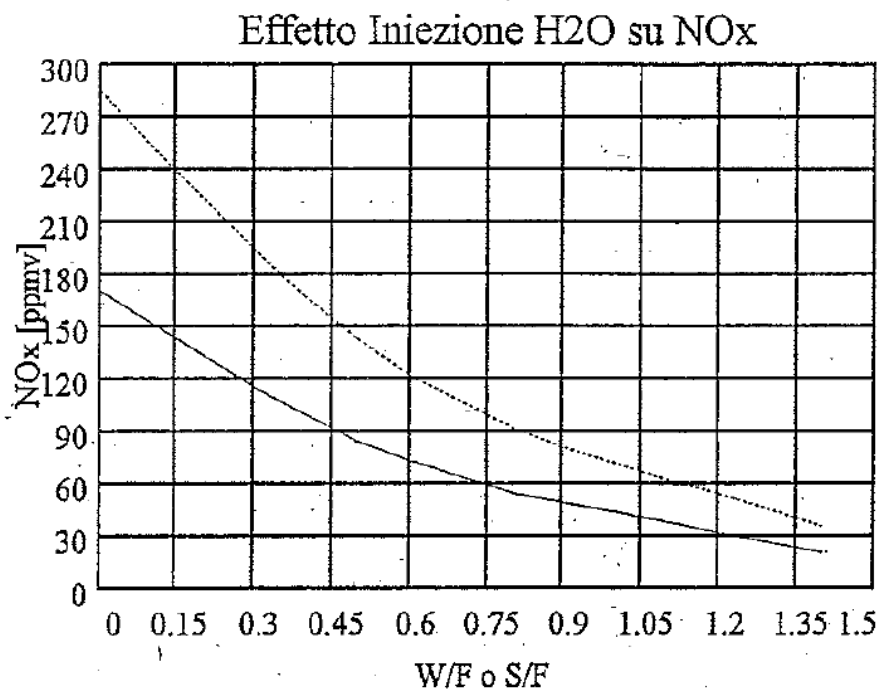


**Figure 5-10** NOx normalized emissions at 60% of Humidity. The continuous line is for Natural Gas, the dash-dot line for liquid fuel.

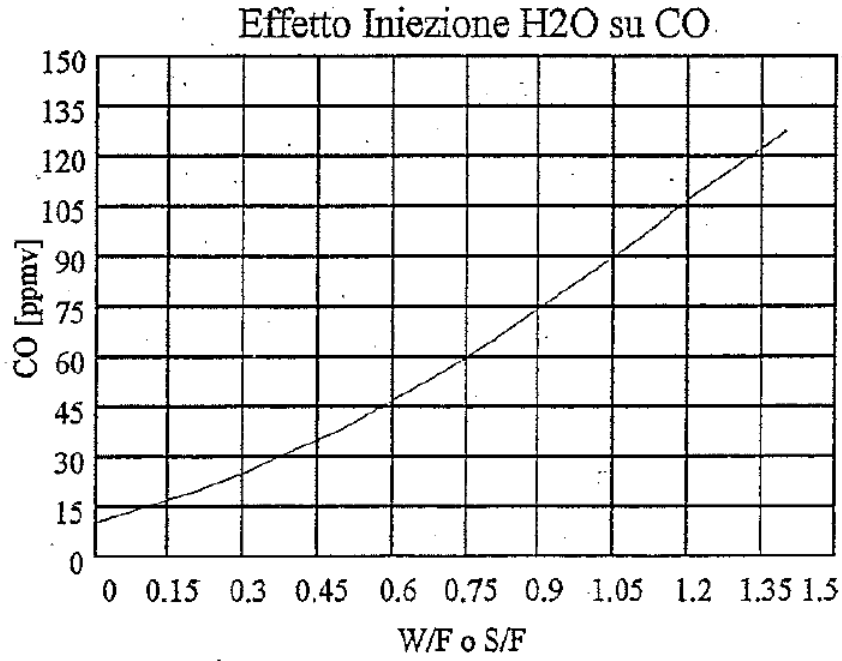


Figure 5-11 CO normalized emissions at 60% of Humidity for Natural Gas

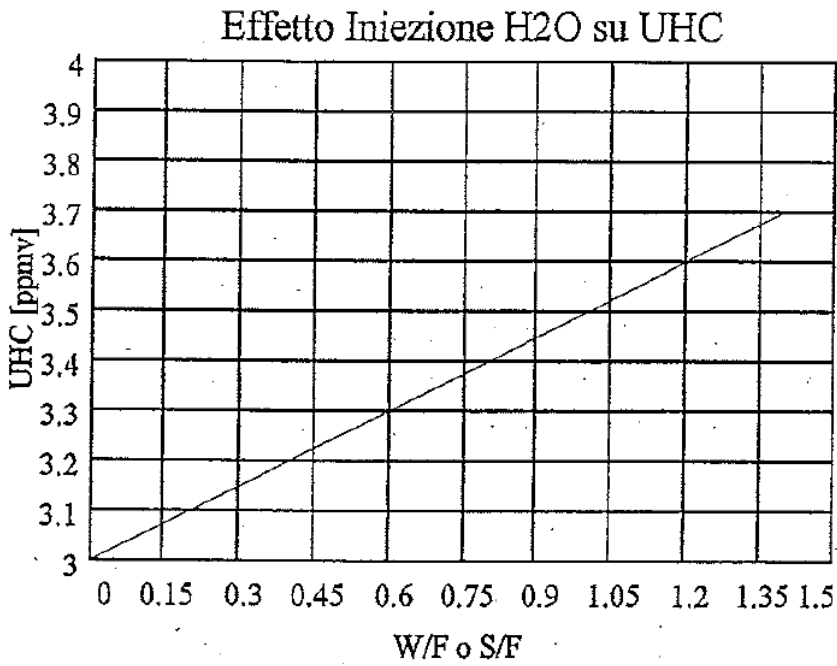


Figure 5-12 UHC normalized emissions at 60% of Humidity for Natural Gas

In **Table 5-1** are reported the normalized and final experimental values for each pollutant:

	NORMALIZED VALUE [ppm]	FINAL VALUE [kg/s]
NOx	170	1.6E-03
CO	10	9E-05
UHC	3	1.5E-05

*Table 5-1 Pollutant normalized and final experimental values*

## 5.5 RESULTS

In this paragraph are presented and compared the simulation results obtained using the SAGE and the FGM combustion models, and then they are compared with the experimental ones. These results have been obtained using CONVERGE for 2D plots and Tecplot360 for 3D plots [13]. The two combustion models have been developed using the same case setup.

The first parameter to be analyzed is the temperature. It is possible to see on the 2D plot, in **Figure 5-13**, the mean temperature for Region 0, which corresponds to the combustion area. The mean temperature is different between the two models in the first 5000 cycles, in particular there is a difference of 200 K in the stable value. Then the mean temperature in the FGM model starts to increase and finally it reaches the SAGE value.

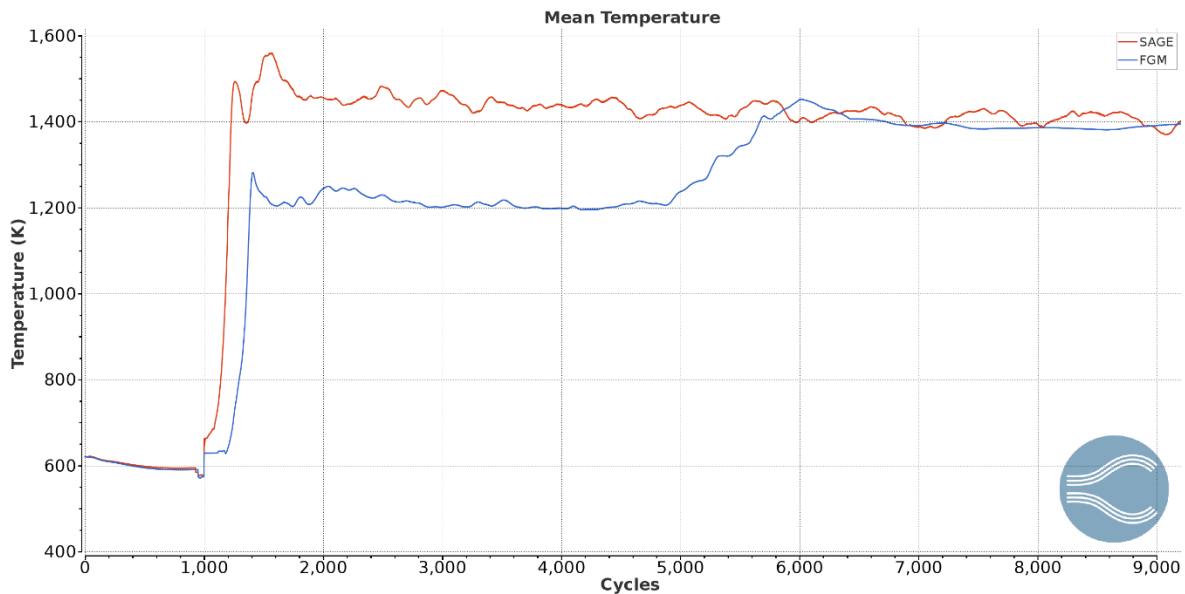


**Figure 5-13** Mean Temperature comparison between SAGE (red) and FGM (blue) models in Region 0.

The two models are characterized by the typical combustion evolution. It is possible to detect the primary, the intermediate and the dilution zone. The temperature profile in the two cases is similar. It is also possible to observe the presence of the toroidal reversal vortex, which will guarantee the continuous alimentation of the combustion. It is also important to observe the effect of the dilution holes and cooling channels on the temperature, which will preserve the combustor from irreparable damages and will guarantee a lower outflow temperature. It is important to maintain a lower outflow temperature to avoid damages at the entrance of the turbine and on the transition piece. Unfortunately, the combustion is starting near the swirler with a M shape. These two conditions are critical for the swirler resistance and they are connected to the geometry of the combustor. Moreover, is also presented, in **Figure 5-17**, the FGM temperature profile at 3000 cycles. As is it possible to see, the combustion is moved up.

In **Figure 5-14**, **Figure 5-15**, **Figure 5-16** is possible to check the differences in combustion and in the **Figure 5-18** are reported the fluid vector evolutions in the primary zone.

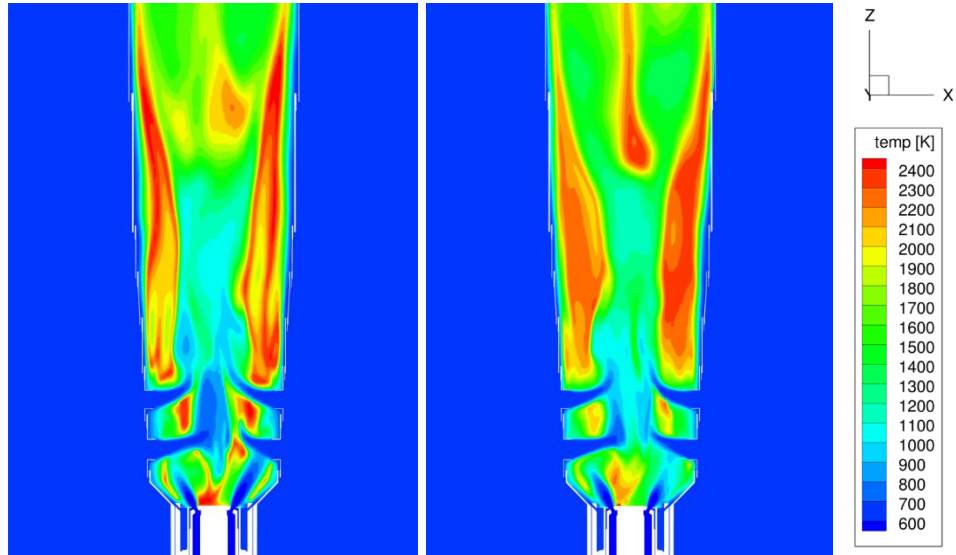


**Figure 5-14** Comparison between SAGE (left) and FGM (right) temperature profiles at 8500 cycles.

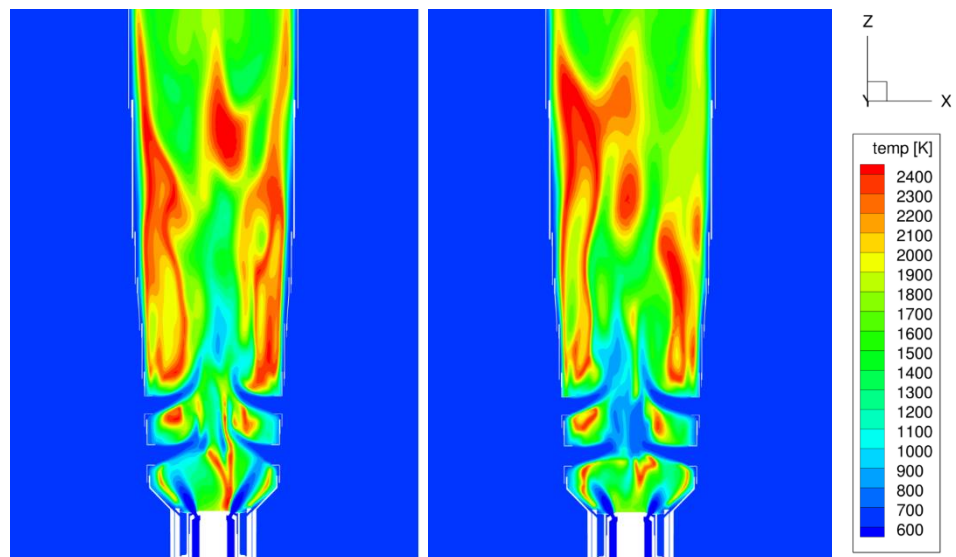


**Figure 5-15** Comparison between SAGE (left) and FGM (right) temperature profiles at 8750 cycles.

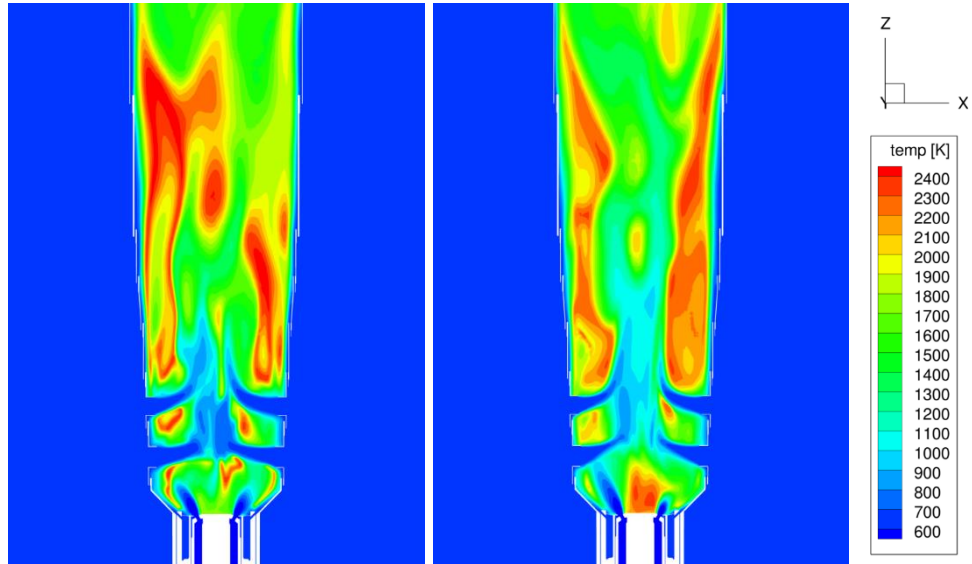


*Figure 5-16 Comparison between SAGE (left) and FGM (right) temperature profiles at 9000 cycles.*

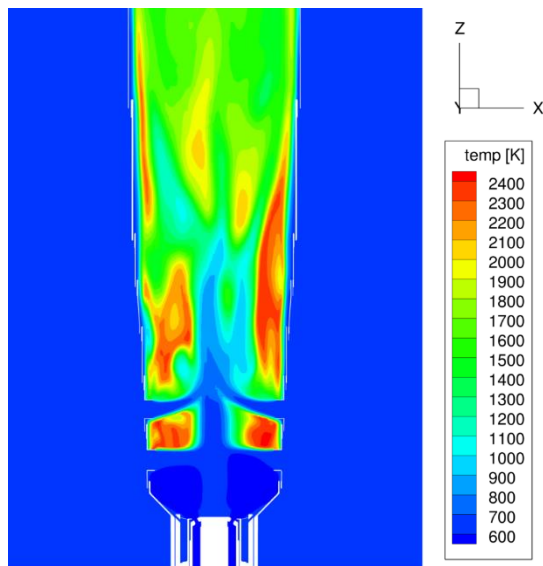


*Figure 5-17 FGM temperature profile at 3000 cycles.*

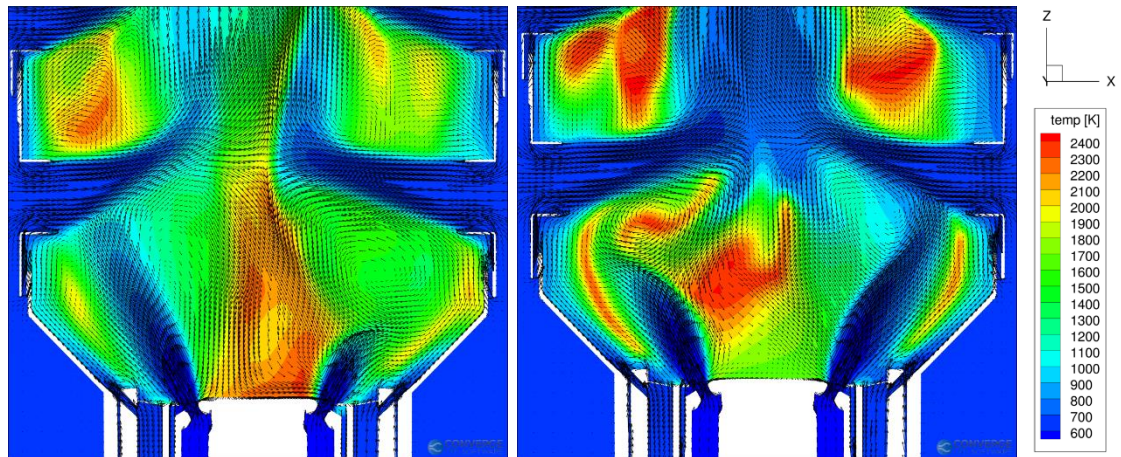


**Figure 5-18** Comparison between SAGE (left) and FGM (right) temperature profile vectors at 9250 cycles.

The second parameter is the equivalence ratio. The analysis of this parameter is fundamental in order to understand the motivations behind the behavior of the FGM model. In fact, as it is possible to see in **Figure 5-20**, the value of the equivalent ratio in the mixing area for the FGM case in the first 5000 cycles is higher than the rich limit of combustion. This means that the fuel is not well mixed with air and the combustion is not starting. This value can be observed also in the SAGE model, but in the external part of the combustion primary zone the equivalence ratio is inside the limits of combustion. In this way the combustion can start and be alimented thanks to the toroidal reverse vortex. Another role of this vortex is to improve the mixing in the swirl area, in fact in the time evolution is possible to observe a variation in equivalence ratio. Then the FGM model will improve the mixing to obtain a good combustion evolution, as it is possible to see in **Figure 5-19**.

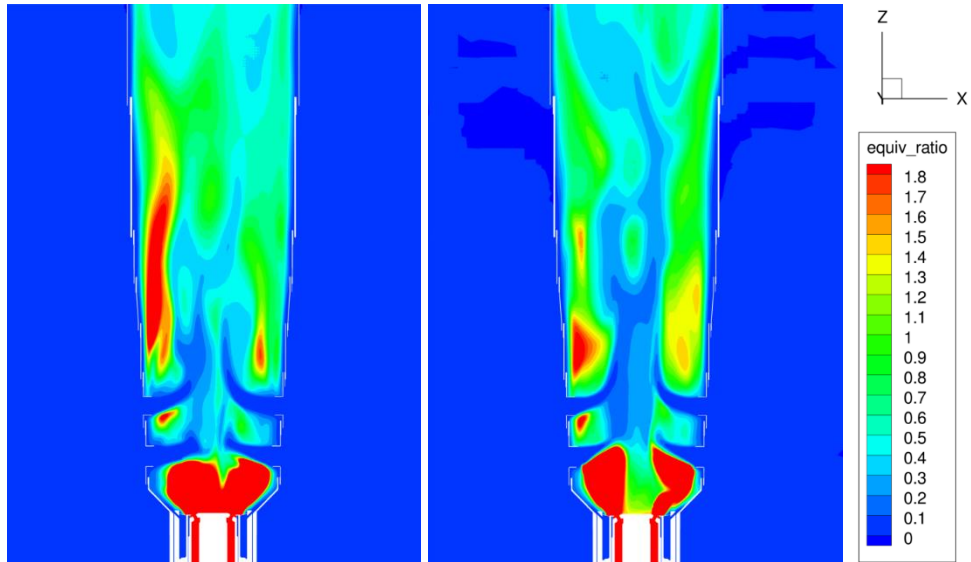


**Figure 5-19** Comparison between SAGE (left) and FGM (right) equivalent ratio profiles at 9000 cycles.

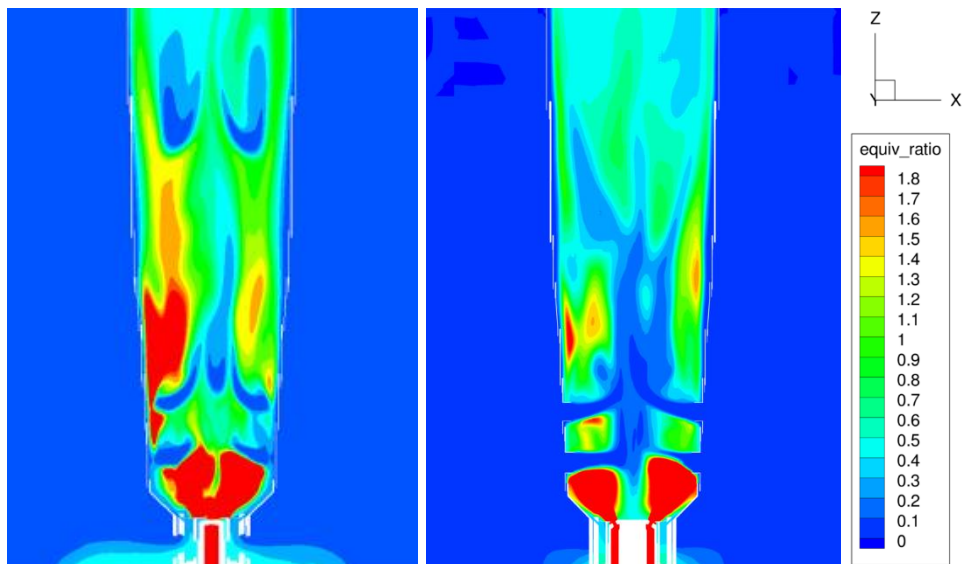


**Figure 5-20** Comparison between SAGE (left) and FGM (right) equivalent ratio profiles at 3000 cycles.

Referring on the pressure, apart from the initial peak, which is the one connected to the energy source release and so to the ignition, the behavior results to be the same, as shown in **Figure 5-21**.

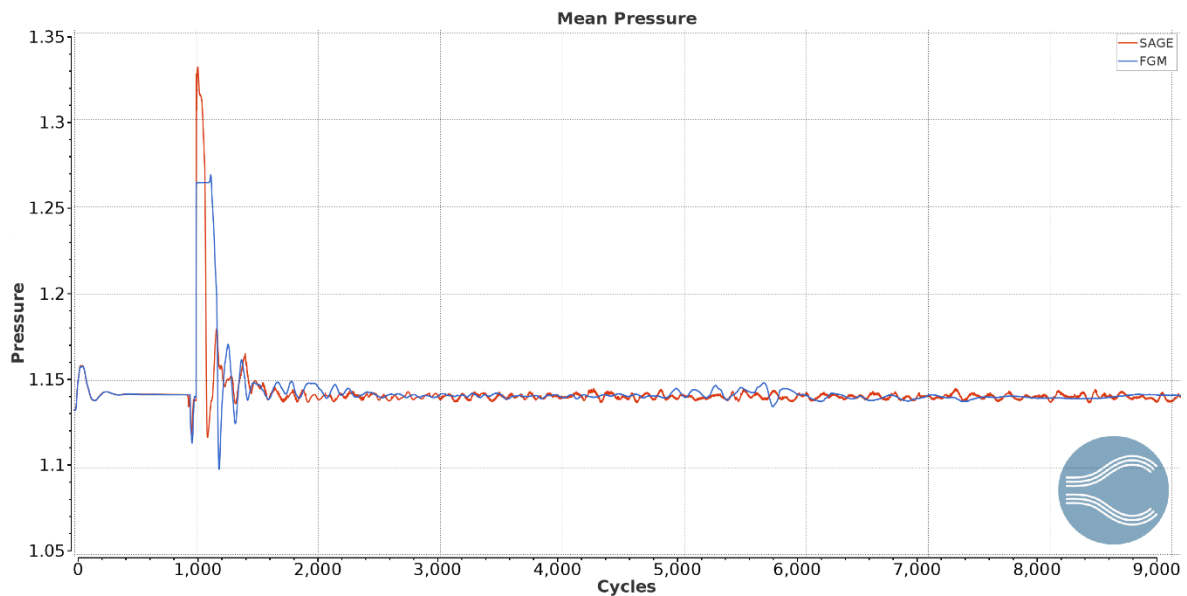


*Figure 5-21 Mean Pressure comparison between SAGE (red) and FGM (blue) models in Region 0. The pressure is measured in bar*

Another parameter to be compared is the velocity magnitude. The SAGE and FGM profiles are very similar, during the entire simulation. The velocity is increasing along the burner thanks to the combustion phenomenon and to the pression of the fresh air, which is entering from the liner holes, on the burned gasses.

In **Figure 5-22** the comparison between the two profiles can be observed.

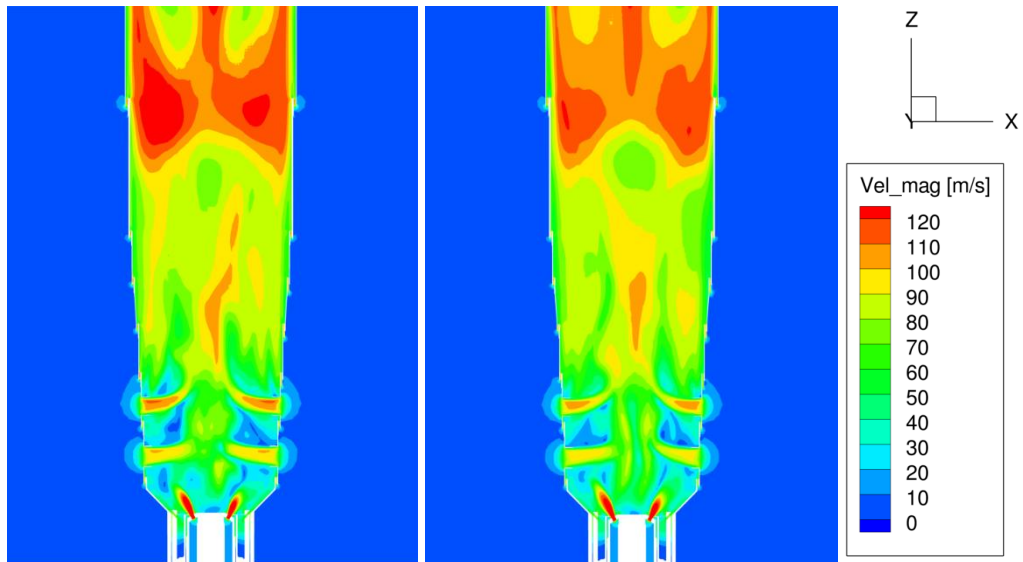


*Figure 5-22 Comparison between SAGE (left) and FGM (right) velocity profiles at 9000 cycles.*

The last parameter that has been checked is the turbulence. It is directly connected to the mixing, which is the main suspect for the differences between the two models. The comparison, in **Figure 5-23** and in **Figure 5-24**, shows that the difference between the two models in the first 5000 cycles is about one order of magnitude. Initially, the SAGE model is characterized by a higher turbulence, which will immediately guarantee a good mixing and will consequently promote the start of the combustion and its continuous alimentation. This behavior is connected to the difficulties of FGM model in transition phase, like the ignition, since FGM is a simplified model, with a simplified interaction between combustion model and turbulence. For this reason, it requires more time to stabilize and give correct results.

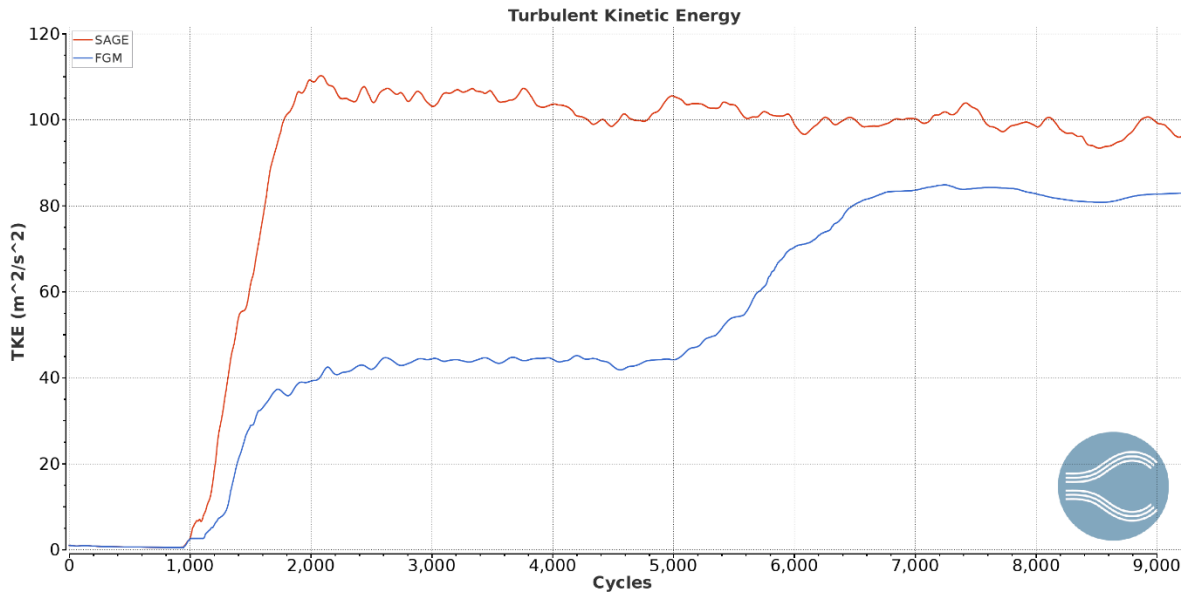


**Figure 5-23** Turbulent Kinetic energy comparison in Region 0. In red the SAGE results, in blue the FGM ones.

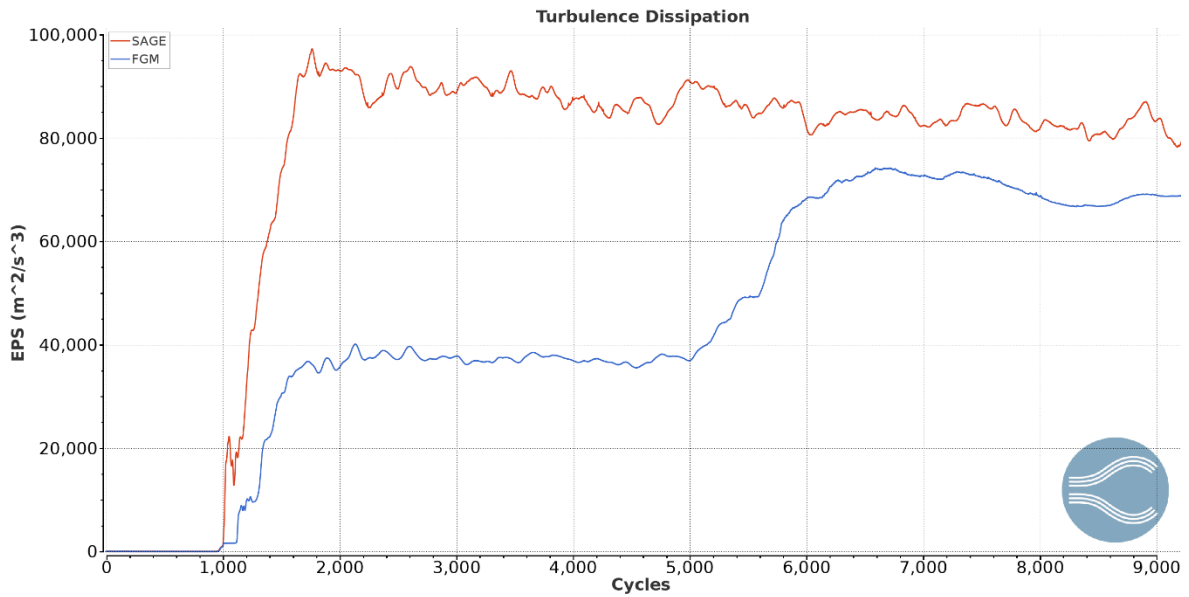


**Figure 5-24** Turbulence dissipation comparison in Region 0. In red the SAGE results, in blue the FGM ones.

Anyways, the aim of this project is to study the pollutant emissions produced by a methane/air mix combustion in steady state conditions. For this reason, the FGM model results to be acceptable as well as the SAGE one. The main difference between the two models is the computational time. In fact, using 32 cores with 8 Gb

for each core, the time needed to complete the simulation reach 9000 cycles is 4-5 days for FGM, against 6-7 days of SAGE.

Now the comparison between simulation results and experimental data can be performed. As said in the **paragraph 5.4**, information about NO<sub>x</sub>, CO and UHC are given. Consequently, the pollutant emissions have been derived from CONVERGE. For the two models, the simulation has been stopped only after it has reached a stability in results. In order to be consistent, the FGM and the SAGE models simulation have been stopped at the same time step. The plots in **Figure 5-25**, in **Figure 5-26** and in **Figure 5-27** show the values. The values have been derived in the outlet boundary, called “exit”, described in **paragraph 5.3**. It is important to note that the experimental result given by EthosEnergy are obtained at the outlet of the turbine [18] using an handheld combustion analyzer. The working principle of the analyzer is presented in [19].

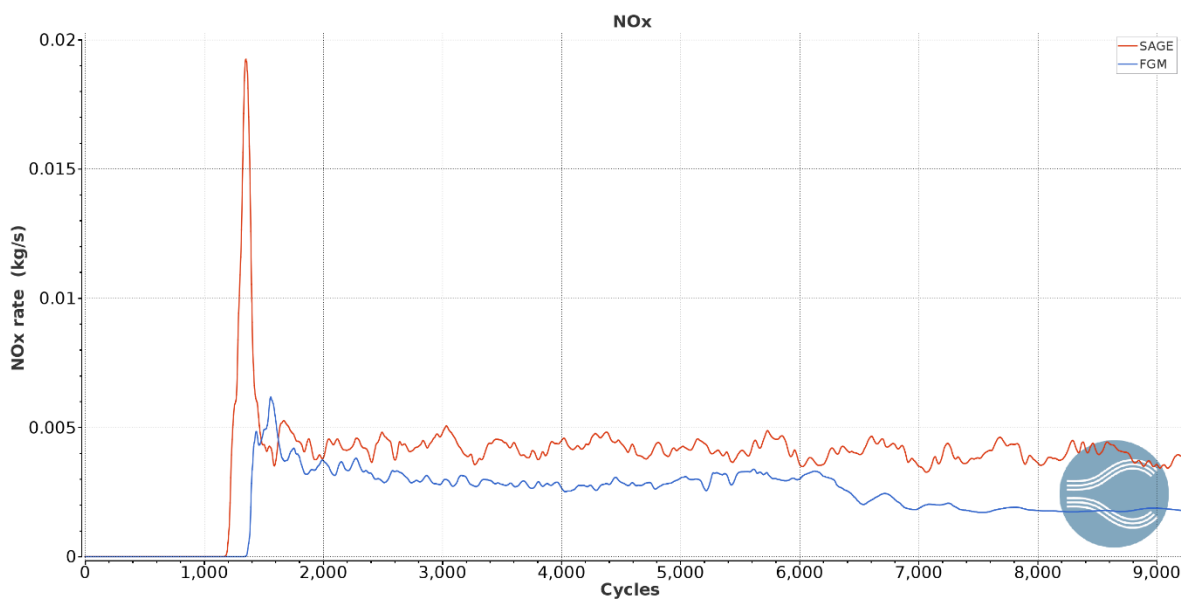


**Figure 5-25** NO<sub>x</sub> emissions comparison, evaluated at the outlet. In red the SAGE results, in blue the FGM ones.

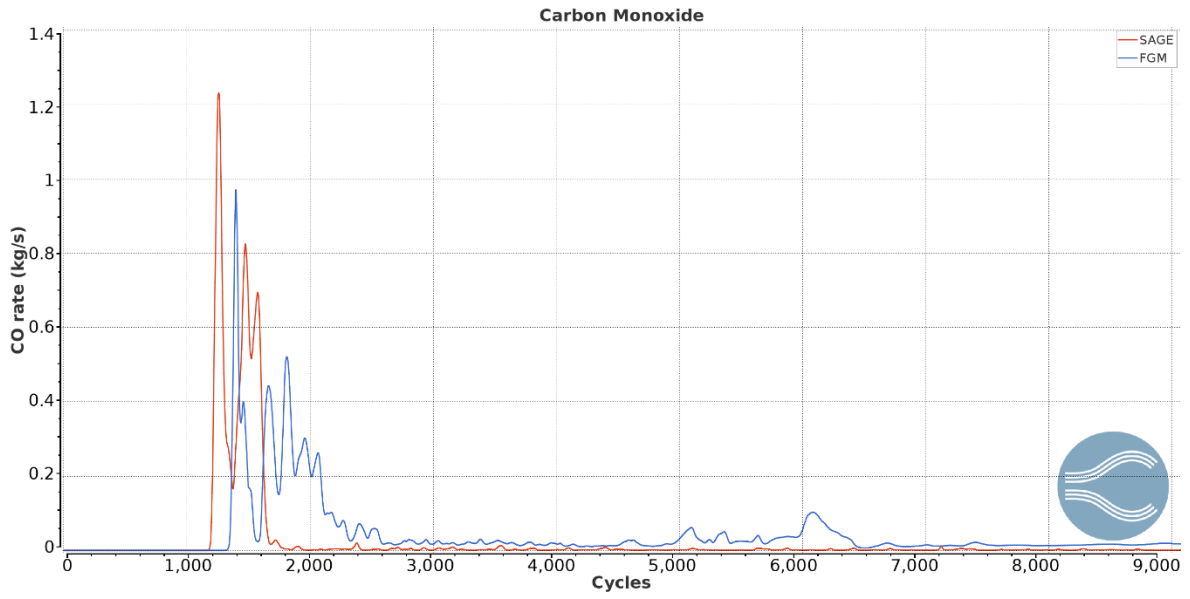


**Figure 5-26** CO emissions comparison, evaluated at the outlet. In red the SAGE results, in blue the FGM ones.

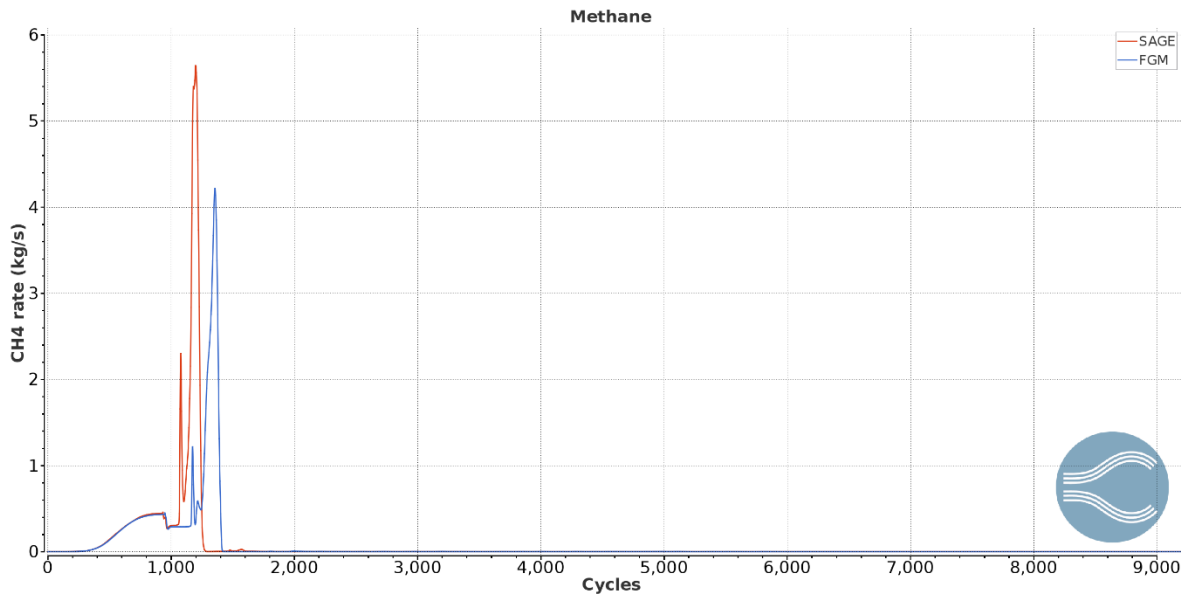


**Figure 5-27** CH4 emissions comparison, evaluated at the outlet. In red the SAGE results, in blue the FGM ones.

The CO mass flow will decrease inside the turbine thanks to the post combustion phenomena, which will not influence the NOx or UHC mass flow. In fact, NOx needs a very high temperature to complete the reactions, like the one inside the combustor. The temperature inside the turbine is more or less 1000 K lower than the maximum one in the combustor. For this reason, the NOx reactions are frozen, and the value found at the outlet of the combustor is equal to the one at the outlet of the turbine. Concerning the UHC formation, they are mostly composed by CH<sub>4</sub>, which will be detected at the outlet because of the amount of fuel that is not burning. The CH<sub>4</sub> needs a high amount of energy to start to burn. This energy is given only by a flame and for this reason, the fuel mass flow that is not burning will not start to burn inside the turbine. This last point is also fundamental in order to avoid peaks of temperature inside the turbine, which will damage it. These post combustion phenomena will decrease the CO mass flow, which does not need a flame to start the oxidation process. The decrease is from one to three orders of magnitude, giving the possibility to validate all the experimental results. In fact, apart from the final values, which are different respect on the experimental data because of the differences in geometry and because of the simplifications due to the combustion, the chemical and the turbulence models, the order of magnitude of each pollutant results to be the same.

Are also presented the variations of NOx and CO profiles in time. It is interesting to check the correspondences between temperature, equivalence ratio and pollutant profiles. In fact, the temperature is higher where the NOx amount increases. Moreover, in the points in which the equivalence ratio is too high to let the combustion start, the CO produced are at the highest value. The complete analysis is for these reasons consistent with the theory behind.

[kg/s]	Experimental data	SAGE results	FGM results
NOx	1.6E-03	3E-03	1.8E-03
CO	9E-05	2.1E-04	1.8E-02
UHC	1.5E-05	2.2E-05	6.2E-06

*Table 5-2 Emissions comparison*

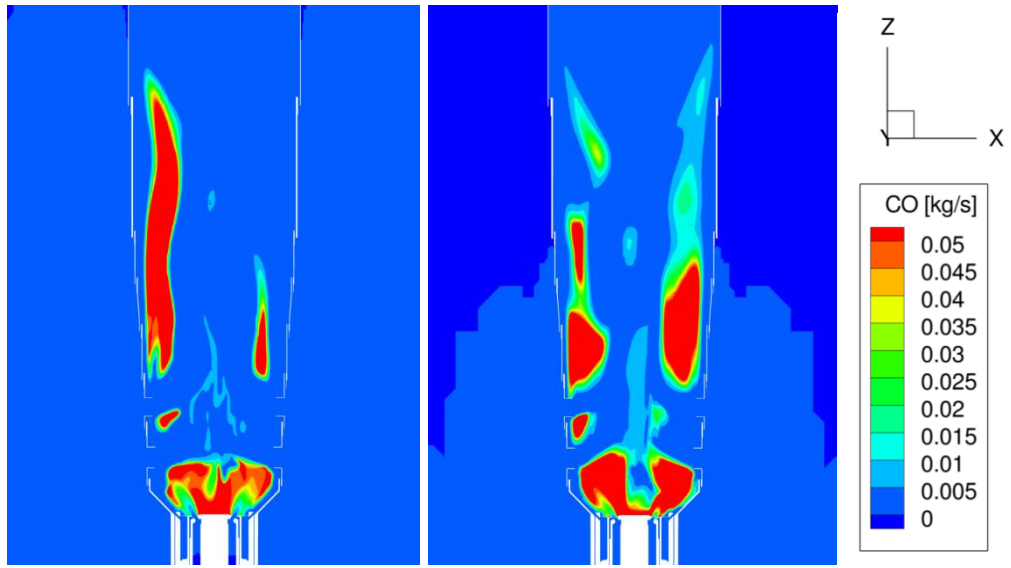


**Figure 5-28** CO formation in SAGE (left) and FGM (right) models at 9000 cycles

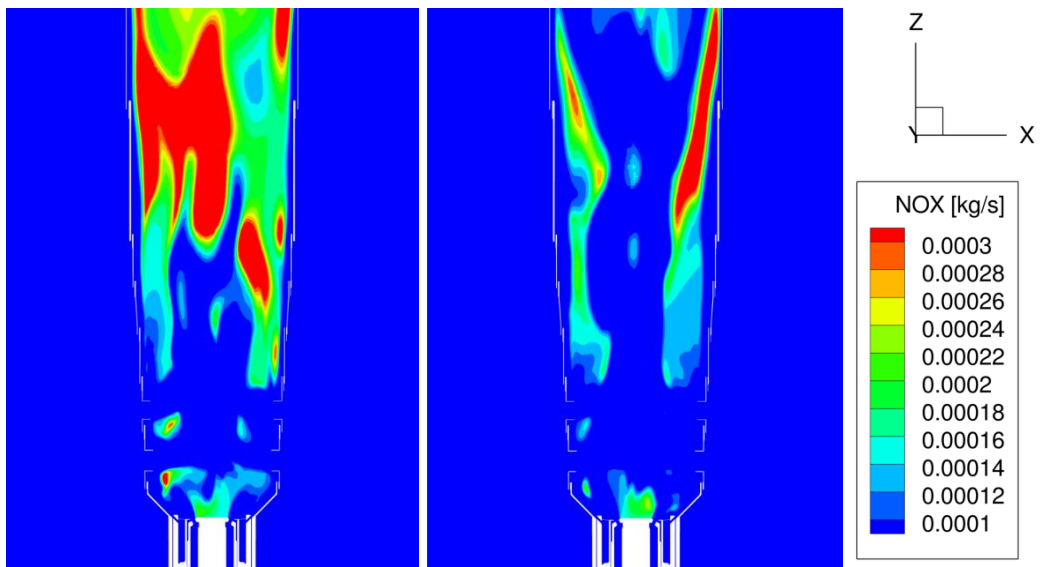


**Figure 5-29** NOx formation in SAGE (left) and FGM (right) models at 9000 cycles

Another comparison can be performed on the mesh. It is possible to check the mesh variations given by the AMR and fixed embedding tools. The initial base grid is of 40 mm and the minimum one is of 5 mm. In the SAGE model the mesh results to be uniform inside the combustion zone, differently from the FGM one, in which there are some internal cells with a mesh of 10 mm. This difference can influence the accuracy of combustion and so of final results. In the figures below is reported the 3D comparison.

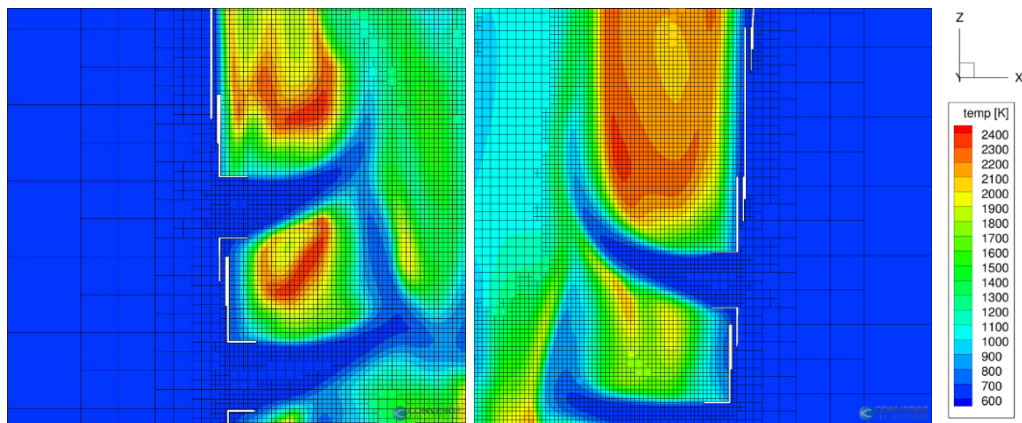


*Figure 5-30 Mesh comparison between SAGE (left) and FGM (right) models at 9250 cycles.*

Finally, have been evaluated the mean values of temperature, velocity and pressure at the outlet of the combustor, and then compared with the information at the inlet of the turbine. This operation has been performed through an integration of these parameters on the exit boundary surface. The results are the following:

	Real	SAGE	FGM
Temperature [K]	1400	1520	1521
Pressure [bar]	1.33	1.33	1.33

*Table 5-3 Real, SAGE and FGM mean values comparison*



# 6 CONCLUSIONS AND FUTURE DIRECTIONS

## 6.1 CONCLUSIONS

In this project, a steady state CFD analysis of an industrial gas turbine combustor has been developed. Firstly, the 3D model of the TG20 combustor has been produced. Then the geometry has been fixed with the CONVERGE diagnostic tool, in order to avoid problems in simulation start. The boundary and consequently the boundary conditions have been defined and then the case setup has been completed. Two different combustion models have been chosen, SAGE and FGM, keeping the same chemical mechanism, turbulence model and case setup, and the results have been compared. The chemical mechanism used is GRI-Mech 3.0, the turbulence model is the RANS RNG k- $\epsilon$ .

The mesh base grid is also the same for the two models, 40 mm. Then, thanks to the AMR and fixed embedding tool, useful to modify the mesh in time and space, it decreases to 5 mm in the combustion zone.

The two models result to be calibrated and the pollutant results are consistent with the experimental ones. The SAGE model requires almost one week to complete the simulation and reach the results stability, using 32 cores, with 8 Gb for each core.

The FGM model requires 4-5 days to reach 9000 cycles and the simulation stability, with the same number of cores, against 6-7 days for SAGE. Moreover, the FGM model results to be more precise in NO<sub>x</sub> evaluation, and almost equally precise in UHC evaluation. For what concern the CO pollutant emissions, the results can't be directly compared with the experimental ones, but in the two cases, thanks to the post combustion phenomena, the results are acceptable.

## 6.2 FUTURE DIRECTIONS

The FGM model, despite the problems in the first part of the simulation, results to be the faster one to perform this kind of CFD analysis. A better calibration of the model must be reached, in order to avoid a step-mean temperature and inconsistency of results, decreasing the simulation computational time of about 1-2 days. After the model re-calibration, it will be necessary to introduce vapor water to decrease the NO<sub>x</sub> emissions, following the curve in **Figure 5-10**. Another task will be to find new geometry solutions, in order to have a better combustion shape and then decrease the NO<sub>x</sub> emissions to reach the standard limits. Another step can be to test other fuels, like Hydrogen or Hythane.



## 7 TABLES INDEX

<b>Table 2-1</b> RNG k- $\epsilon$ constants and relative value .....	29
<b>Table 5-1</b> Pollutant normalized and final experimental values .....	89
<b>Table 5-2</b> Emissions comparison .....	100
<b>Table 5-3</b> Real, SAGE and FGM mean values comparison .....	102



# 8 FIGURES INDEX

<b>Figure 1-1</b> Section view of FIAT TG20, courtesy of EthosEnergy.....	10
<b>Figure 1-2</b> A SGT-100 Siemens gas turbine [2].....	11
<b>Figure 1-3</b> Schematic of the Brayton Cycle [3].....	12
<b>Figure 1-4</b> p-V and T-s diagram for Brayton Cycle .....	12
<b>Figure 2-1</b> Turbulent kinetic energy spectrum .....	23
<b>Figure 3-1</b> Comparison between the traditional CFD and CONVERGE workflow [6]. .....	31
<b>Figure 3-2</b> Sample three-cell, one-dimensional spatial domain [5]. .....	33
<b>Figure 3-3</b> CONVERGE solution procedure [5]. .....	35
<b>Figure 3-4</b> A regular cell combined with a cut-cell [5] .....	40
<b>Figure 3-5</b> Cell Pairing [5].....	40
<b>Figure 3-6</b> A visualization of Boundary embedding around a valve [5].....	42
<b>Figure 3-7</b> A grid generated using nozzle embedding [5] .....	43
<b>Figure 3-8</b> Evolution in time of a combusting spray bomb [5] .....	44
<b>Figure 4-1</b> Example of gas turbine combustor, by Rolls Royce [8]. .....	53
<b>Figure 4-2</b> Section of the three main combustor types [7]. .....	54
<b>Figure 4-3</b> Turboannular combustor arrangement [7]. .....	55
<b>Figure 4-4</b> Two basic examples of (a) aerodynamic and (b) bump diffusers [7]. .	57
<b>Figure 4-5</b> Main components of a conventional combustor [7]. .....	58
<b>Figure 4-6</b> Example of flow pattern for a generic combustion chamber [9].....	60
<b>Figure 4-7</b> Complete view and section view of the injector-swirler, courtesy of EthosEnergy.....	61
<b>Figure 4-8</b> Flammability limits of methane [10]. .....	65
<b>Figure 4-9</b> Example of combustion chamber stability loop [7]......	66
<b>Figure 4-10</b> Influence of pressure in the stability loop [7]. .....	67
<b>Figure 4-11</b> Water injection rigs for stability tests [7]. .....	68
<b>Figure 4-12</b> Typical water injection stability loop [7]. .....	69
<b>Figure 4-13</b> Example of primary zone for tubular (a) and annular (b) combustors [7]. .....	71
<b>Figure 5-1</b> Initial geometry, courtesy of EthosEnergy .....	75
<b>Figure 5-2</b> Simplified geometry.....	75

<b>Figure 5-3</b> STL file of the final geometry. The section has been performed only on the casing. ....	77
<b>Figure 5-4</b> Complete view of the dilution, mixing and cooling holes on the liner..	78
<b>Figure 5-5</b> Detail of the cooling channels. ....	78
<b>Figure 5-6</b> Back and front view of injector-swirler. ....	79
<b>Figure 5-7</b> Example of Nonmanifold edge (red line) and problem resolution (a) [5]. .....	80
<b>Figure 5-8</b> Example of Intersecting triangles (red lines) and problem resolution (a) [5]. .....	81
<b>Figure 5-9</b> Example of Overlapping triangles [5]. ....	81
<b>Figure 5-10</b> NOx normalized emissions at 60% of Humidity. The continuous line is for Natural Gas, the dash-dot line for liquid fuel. ....	87
<b>Figure 5-11</b> CO normalized emissions at 60% of Humidity for Natural Gas .....	88
<b>Figure 5-12</b> UHC normalized emissions at 60% of Humidity for Natural Gas .....	88
<b>Figure 5-13</b> Mean Temperature comparison between SAGE (red) and FGM (blue) models in Region 0. ....	90
<b>Figure 5-14</b> Comparison between SAGE (left) and FGM (right) temperature profiles at 8500 cycles. ....	91
<b>Figure 5-15</b> Comparison between SAGE (left) and FGM (right) temperature profiles at 8750 cycles. ....	91
<b>Figure 5-16</b> Comparison between SAGE (left) and FGM (right) temperature profiles at 9000 cycles. ....	92
<b>Figure 5-17</b> FGM temperature profile at 3000 cycles. ....	92
<b>Figure 5-18</b> Comparison between SAGE (left) and FGM (right) temperature profile vectors at 9250 cycles. ....	93
<b>Figure 5-19</b> Comparison between SAGE (left) and FGM (right) equivalent ratio profiles at 9000 cycles. ....	94
<b>Figure 5-20</b> Comparison between SAGE (left) and FGM (right) equivalent ratio profiles at 3000 cycles. ....	94
<b>Figure 5-21</b> Mean Pressure comparison between SAGE (red) and FGM (blue) models in Region 0. The pressure is measured in bar .....	95
<b>Figure 5-22</b> Comparison between SAGE (left) and FGM (right) velocity profiles at 9000 cycles. ....	96

<b>Figure 5-23</b> Turbulent Kinetic energy comparison in Region 0. In red the SAGE results, in blue the FGM ones.....	97
<b>Figure 5-24</b> Turbulence dissipation comparison in Region 0. In red the SAGE results, in blue the FGM ones.....	97
<b>Figure 5-25</b> NOx emissions comparison, evaluated at the outlet. In red the SAGE results, in blue the FGM ones.....	98
<b>Figure 5-26</b> CO emissions comparison, evaluated at the outlet. In red the SAGE results, in blue the FGM ones.....	99
<b>Figure 5-27</b> CH4 emissions comparison, evaluated at the outlet. In red the SAGE results, in blue the FGM ones.....	99
<b>Figure 5-28</b> CO formation in SAGE (left) and FGM (right) models at 9000 cycles .....	101
<b>Figure 5-29</b> NOx formation in SAGE (left) and FGM (right) models at 9000 cycles .....	101
<b>Figure 5-30</b> Mesh comparison between SAGE (left) and FGM (right) models at 9250 cycles. ....	102



## 9 BIBLIOGRAPHY

- [1] EthosEnergy, "EthosEnergy Group."
- [2] Siemens, "Siemens Gas Turbine."
- [3] Y. A. Cengel, "Thermodynamic, an engineering approach."
- [4] A. Donini, "Advanced Turbulent Combustion Modeling for Gas Turbine Application," 2014.
- [5] M. S. CONVERGECFD and M. Series, "CONVERGE Manual, CONVERGE CFD 2.3," no. May, 2016.
- [6] CONVERGECFD, "CONVERGECFD Software."
- [7] A. . Fallis, *GAS Turbine Combustion, Alternative Fuels and Emissions*, vol. 53, no. 9. 2013.
- [8] R. Royce, "Rolls Royce Gas Turbine."
- [9] Aeromodelbasic, "Combustion Process."
- [10] R. M. Hartmann, "Flammability limit of Methane."
- [11] PTC, "Pro/ENGINEER."
- [12] Z. Q. Gregory P. Smith, David M. Golden, Michael Frenklach, Nigel W. Moriarty, Boris Eiteneer, Mikhail Goldenberg, C. Thomas Bowman, Ronald K. Hanson, Soonho Song, William C. Gardiner, Jr., Vitali V. Lissianski, "GRI-mech 3.0."
- [13] T. Products, "Tecplot360."
- [14] L. M. in P. Politecnico di Torino, "Lab Diesel, Propulsori termici," pp. 1–7, 2018.
- [15] R. P. Settore Sviluppo Energetico Sostenibile, "RISPOSTA ALLE DOMANDE DEGLI OPERATORI SUL NUOVO CATASTO PER GLI IMPIANTI."
- [16] L. S. Diego Lentini, Università degli studi di Roma, "Modellistica della combustione turbolenta e controllo delle emissioni di inquinati."
- [17] S. consulenza Centro Analisi Biochimiche, "NOx measurement corrections."
- [18] C. E. D. EthosEnergy, "EN006-18 M251B8 Combustor System Failure Root Cause Analysis EN006-18," 2018.

[19] Seitron, "Combustion Analyzer."



## **Acknowledgements**

È arrivato anche per me il momento dei ringraziamenti. Mi piace pensare che non sia solo “usanza” ringraziare chi mi è stato accanto in questo progetto, poiché queste parole sono tanto sincere quanto necessarie. Vorrei prima di tutto ringraziare i miei relatori, Daniela Misul e Mirko Baratta, per il continuo supporto e le belle parole che mi hanno sempre fatto sentire all'altezza di questo progetto. Altrettanto importanti sono stati Prashant, Mohsen e Silviu. Sono sempre stato un “solitario” dal punto di vista dello studio, ma grazie a voi sono riuscito a capire quanto fosse fondamentale l'impatto di un gruppo preparato e con grandi obiettivi. Non passa di certo in secondo piano l'intero gruppo di laboratorio, perché anche nei momenti più pesanti si riusciva a ridere e scherzare come se niente fosse. Ringrazio il team di EthosEnergy, che tra aperitivi e partite di calcetto è riuscito a rendere il mondo del lavoro un po' meno spaventoso (anche se insomma, chi non vorrebbe vivere da mantenuto?). Una menzione speciale a Giovanni Attanasio, il mio disegnatore preferito.

Ringrazio tutti i miei amici, d'infanzia e non, che poi tanto ormai è come se fossero tutti amici d'infanzia. Siete la mia prima, seconda, e pure terza famiglia, sul serio.

Gli ultimi ringraziamenti sono forse i più importanti (non ve la prendete se non siete qui, ma non potete competere). Sento la necessità di ringraziare tutta la mia famiglia. Grazie mamma, hai sopportato due figli e un marito lontani, hai sopportato i miei sfoghi immotivati su di te, hai sopportato tutte le mie fisse e le mie paranoie. La mia roccia. Grazie papà, sono ormai più di 20 anni che sei via per garantire un futuro importante ai tuoi figli, nonostante le sofferenze e la nostalgia di casa. La soddisfazione più grande spero sarà vedere tutti i tuoi sforzi realizzati. Non te la prendere se quando tornerai i tuoi figli lavoreranno chissà dove, penseremo sempre a te. Grazie Davide, se mi sono sentito a mio agio in questa città è perché in fin dei conti “per qualsiasi cosa c'è tuo fratello”. Che poi magari sono io quello responsabile tra i due, ma se lo sono è solo perché vedo in te una certezza. Sei il figlio più intelligente, l'ho sempre pensato.

Ringrazio i miei zii, i miei cugini e i miei nonni. Avete sempre puntato su di me, aiutandomi a fare quello sforzo in più quando mi sentivo a terra. Grazie.

Ah giusto, dimenticavo la persona più importante: me stesso. Grazie fra!!